DESIGN AND PERFORMANCE OF LARGE AREA SCINTILLATION COUNTERS WITH GOOD ENERGY RESOLUTION

A thesis submitted to the Faculty of Graduate Studies in partial fulfilment of the requirements for the degree of Master of Science.

by

Thomas William Millar

University of Manitoba, Winnipeg

August, 1969

ABSTRACT

Two pairs of large area($88cm^2$ and $520cm^2$) scintillation counters were constructed to detect protons having energies in the range 7mev to 50mev. Some of the properties of the photomultipliers and base circuits which were used with the counters,were studied in order to obtain suitable pulseheights and pulse shapes for use in experiments involving a wire chamber spectrometer. In all of the counters studied the pulseheights were dependent on the position at which the protons entered the scintillators, and this had the effect of decreasing the energy resolution. By finding the distribution of pulseheights across the face of the scintillators it was possible to form a set of calibration points which were used along with position information obtained from the wire chambers to correct for this pulseheight non-uniformity. The energy resolutions at 47mev , with collimators at the centres of the scintillators, were 1.9% for the smaller of the two pairs of counters and 3.5% for the larger. From preliminary data obtained with the larger pair of counters it was possible, using the method described above, to improve the uncollimated energy resolutions by a factor of three from 18% to 6%.

ACKNOWLEDGEMENTS

The author wishes to express his deep appreciation to his Thesis adviser Dr. J.V. Jovanovich, for his constant encouragement and invaluable advice during the course of this study. He also wishes to thank Dr. J.C. Thompson for his assistance in the design of the mountings for the scintillation counters. Thanks also are due to Messrs J. Mckeown, G. Greeniaus, and D. Peterson for their valuable help in the writing of computer programs, and for the many hours they have spent in the collection of the data.

The author would also like to thank Miss K. Ewy for her assistance in the typing of the second draft of the Thesis.

Finally, the author wishes to express his appreciation of the financial support given to him by the University of Manitoba, and the Atomic Energy Control Board of Canada.

TABLE OF CONTENTS

Table of contents-cont.

LIST OF TABLES

LIST OF FIGURES

List of Figures - cont.

CHAPTER I

INTRODUCTION

The object of this work was to construct and test two pairs of scintillator-photomultiplier assemblies for use in a wire chamber spectrometer [1]. The spectrometer was designed and constructed to study some (p,2p) reactions and in particular the proton-proton bremsstrahlung process. Its main advantage over other, more commonly used methods for data collection is that it subtends a very large solid angle (between .1 and .2 steradians) at the target while at the same time maintains very good angular resolution. The energies of the outgoing particles are measured in a pair of scintillation counters which are also used to select the events of interest and to initiate the triggering of the wire chambers. As a result of the large solid angles employed, large area (400 cm^2) scintillators were required.

The distance the light has to travel from the point of scintillation to the photocathode of the photomultiplier in scintillators of the above size is generally very long and, consequently the absorption of light will decrease the resolution. This effect will be reduced by placing the photomultiplier close to the scintillator. Another, more important effect is the decrease in the overall resolution caused by the variation in pulse-height from different positions in the scintillator. It is for the above reasons that two pairs of counters were constructed. In the case of the first pair, or small counters, the scintillators 10.6 cm. in diameter and 2.3 cm. thick are attached directly to the photocathodes of five inch photomultipliers while in the second pair, or large counters, scintillators 22.8×22.8×2.5 cm. are viewed from top and bottom sides by two five inch photomultipliers through 30.5 cm. long light pipes. In both the small and large counters the pulseheight depends on the position at which the scintillation takes place. In the small counter this position dependence is due mainly to photocathode non-uniformities while in the large counter it is due mainly to light absorption in the scintillator. As the precise measurement of the energies of the particles is of great importance we have tried to improve the resolution of the counters by correcting the pulseheight non-uniformity using the information from the wire chambers.

The main features of the spectrometer are shown in Figure 1. In the case of a gaseous target the reaction volume is defined by two sets of baffles in the forward direction and by the beam profile in the other two directions. When a nuclear reaction takes place the two outgoing charged particles which are to be observed pass through a pair of wire chambers and are detected in scintillators S1 and S2 where their energies are measured. If the particles satisfy the coincidence requirement and their energies are in the desired range, the wire chambers are sparked and information

Figure 1

Diagramatical representation of the spectrometer showing scattering chamber, wire chambers WSC1 to WSC4, and scintillation counters S1 and S2. The chamber is filled with the gas to be studied (hydrogen in the case of the proton-proton bremsstrahlung experiment) at atmospheric pressure. Propane and helium jackets are used to separate the helium-neon mixture of the wire chambers from the target gas and to decrease multiple scattering. Two sizes of scintillation counters are shown, a small one 10.6 cm in diameter and 2.3 cm thick (dotted lines), and a large one 22.8 22.8 2.5 cm (heavy lines). The thickness of the wire chambers (6.2 mm) is not shown to scale, and the distance separating them is only approximate.

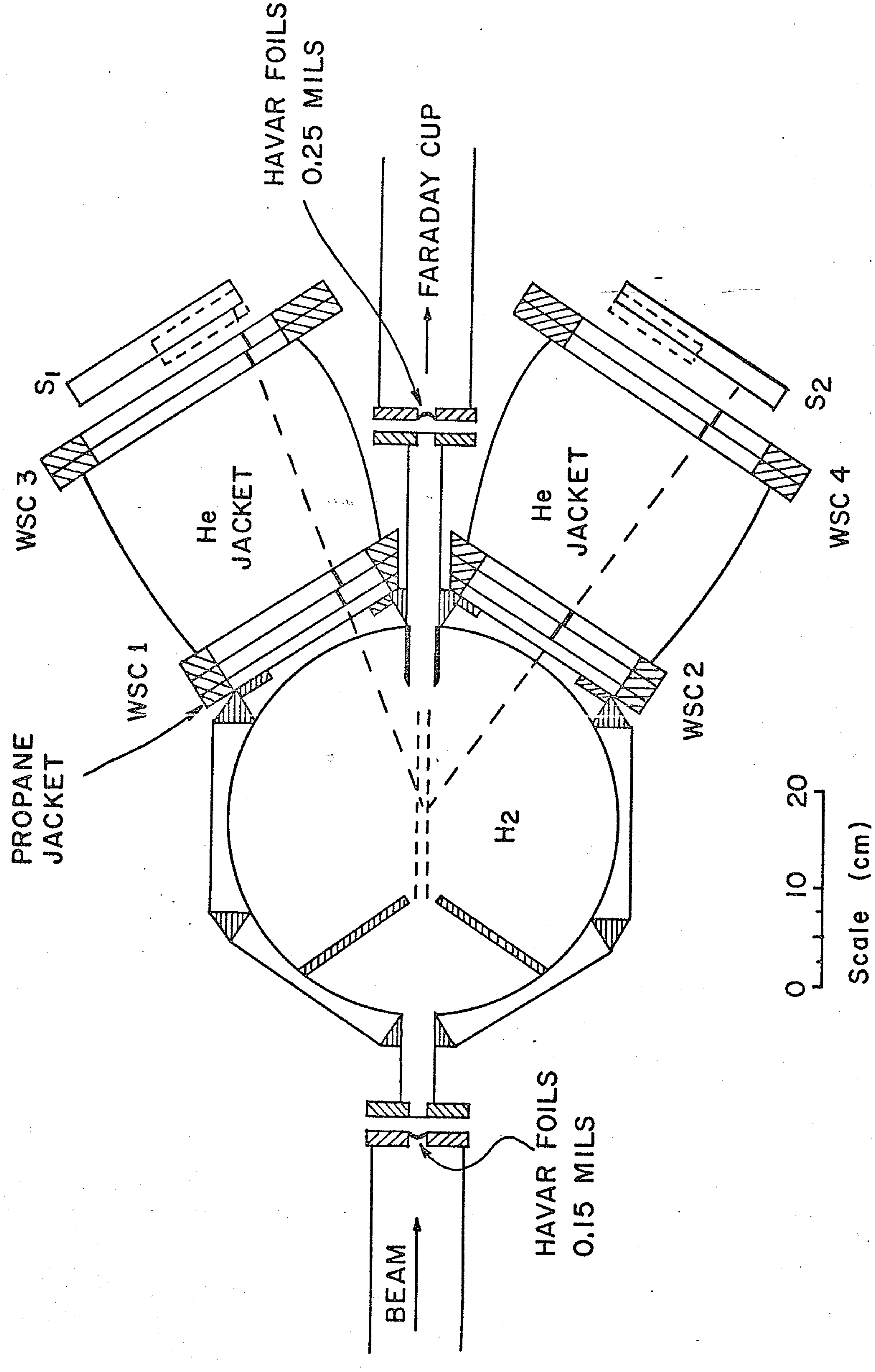
HAVAR FOILS
0.25 MILS
FARADAY CUP
S1
S2
WSC 3
WSC 4
He
JACKET
He
JACKET
WSC 1
WSC 2
PROPANE
JACKET
H2
0
10
20
Scale (cm)
BEAM
HAVAR FOILS
0.15 MILS

Fig.1

yielding their position is subsequently read into two on-line computers (PDP-9 and IBM 360/65). The PDP-9 computer, after decoding this information, calculates the spark co-ordinates, the trajectories of the particles, and determines whether or not they form a vertex lying within the reaction volume. If they do, the event is accepted and the pulseheights and track co-ordinates are transferred to the large computer (IBM 360/65) where the pulseheights are corrected for the non-uniformity and a complete kinematic analysis is performed.

The requirements of the scintillation counters in experiments using the above mentioned wire chamber spectrometer are (1) fast timing information to spark wire chambers and (2) pulseheight information for energy measurements. The timing pulse is taken from the anodes of the photomultipliers and goes through a differential discriminator where it is energy selected and shaped before entering a coincidence unit with the resolving time set at 20 nano-seconds *. One of the restrictions imposed on the anode pulse by the electronics is that the range of energies of interest should have pulseheights between 100 mv and 500 mv. Therefore, in order that all protons with energies between 7 mev and 50 mev are analysed, the anode pulses should be slightly saturated. The analog energy information is obtained by taking pulses from the appropriate dynodes of the phototubes, inverting them by pulsetransformers

* The flight times of two protons detected in the spectrometer may differ by as much as 12 nano-seconds; also the triggering time of the differential discriminators can vary by 6 or 7 nano-seconds as in the case of the small counters (due to the rise time of the pulses).

and sending them via 250 ft long double shielded cables to the control room. There, they are lengthened in a gate and stretcher module (EG&G LG102) and digitised in a pair of Nuclear Data ADC's. The gate opens just before the fast dynode pulses have arrived and closes as soon as they have passed through it, thus gating out the noise produced by sparking the chambers.

It is perhaps worthwhile at this stage to explain what we mean by the energy resolution and the non-uniformity of the counters. The overall resolution, or uncollimated resolution is defined as the full width at half maximum (FWHM) of the distribution of monoenergetic protons striking the entire face of the scintillator, divided by the energy of the protons. This number is then multiplied by 100 and expressed as a percentage. The collimated resolution is defined as above except in this case the monoenergetic protons are collimated so that they strike only a small area of the scintillator. The non-uniformity is given by the following:

$$2.\left(\frac{\text{maximum pulseheight} - \text{minimum pulseheight}}{\text{maximum pulseheight} + \text{minimum pulseheight}} \right).100\%$$

The design and performance of large area scintillation counters employing light pipes to transfer the light from one or more faces of the scintillator to the photocathode of the photomultiplier has been reported by numerous investigators [2-9]. The results for the pulseheight non-uniformity vary from 10% to 40% depending on the geometry of the scintillators and light pipes. In most of the work reported so far, the investigators have been unable to correct for the non-uniformity, and hence, the overall energy resolution of the scintillator has been optimized rather than the collimated resolution at any particular point.

One of the purposes of this work was to correct for the pulseheight non-uniformity of the scintillators by using the position information from the wire chambers along with correction constants, found from a set of calibration points stored in the memory of the computer. The set of calibration points were, in turn, determined by measuring the distribution of pulseheights across the face of the scintillator.

CHAPTER II

SCINTILLATORS AND LIGHT PIPES

2-1 General Considerations

The following series of processes leads to the detection of a scintillation at the anode of a photomultiplier;

1) interaction of charged particles in the scintillator,

11) conversion of energy into light,

111) transfer of light to the photocathode,

1V) emission of photoelectrons from the photocathode,

V) collection of photoelectrons at first dynode, and

V1) multiplication of electrons at subsequent dynodes.

Each of the above processes is statistical in its nature, except number three which depends on the geometry. These processes may be approximated by exponential, poisson and/or gaussian distributions. By convoluting the expressions for the individual processes it is possible to describe analytically the operation of the scintillation counter. From studying the above processes [10-13], the most successful being those using the theory of branching processes developed by Euling [14], valuable information on the energy and time resolution of scintillation counters has been obtained. However, in practice once the scintillation material and photomultiplier have been chosen only the transfer of light to the photocathode and the design of the base circuit for the phototube remains to be considered.

2-2 Light Collection and Uniformity of Counters

Before describing the scintillator-phototube assemblies used with the spectrometer it is worthwhile discussing the factors influencing their design.

2-2.1 Geometrical Considerations for Scintillators with Transparent Walls

When a scintillation takes place in a scintillator having transparent * walls a certain amount of the light (trapped light) is continuously internally reflected from the walls, and may be collected provided one or more faces of the scintillator is optically coupled to a photomultiplier. In order, however for this trapped light to be independent of position at which the scintillation takes place the scintillator should be a parallelopiped [2,15]. In the cases of cylindrical and spherically shaped scintillators with transparent walls, the amount of trapped light collected by the phototube is dependent on position, and hence would not make satisfactory shapes for large area scintillators where the pulseheight uniformity is important [16]. Along with the trapped light the photocathode collects all the direct light within a cone of apex angle, γ_0, equal to the angle of total internal reflection. For this direct light to be also independent of position the scintillation must take place at a distance greater than the lengh, $L = d.\tan\gamma_0$ from the photosensitive surface, where d equals the diagonal of the face being viewed [2]. This position effect may be eliminated

* The scintillators are made so as to have either 'transparent' or'diffused' walls. If the walls are highly pollished they are called transparent, and if they are made rough and coated with a reflective paint they are called diffuse.

provided a light pipe of length L is connected between the scintillator and the photosensitive surface. The light pipe may be considered, as far as calculations are concerned, as part of the scintillator. In practice however, light pipes will only approximately satisfy this condition. A simple calculation, similar to that given by Akimov,[12] for the light collected by a phototube coupled to one face of a scintillator is as follows:

Neglecting the absorption of light in the scintillator and light pipes, the amount of light from a point in the scintillator incident on an element of solid angle $d\Omega$ is

$$dR = \frac{d\Omega}{4\pi} = \tfrac{1}{2}\times \sin\gamma\, d\gamma$$

hence, the amount of light within a cone of apex angle γ_0, equal to the angle of total internal reflection, will be given by;

$$R_c = \int_0^{\gamma_0} dR = \tfrac{1}{2}\times(1 - \cos\gamma_0)$$

From any point inside a parallelopiped scintillator six such cones can be constructed with axis perpendicular to the faces of the scintillator, consequently, the percentage of the total amount of light collected from one face is;

$$R = 100\times(1 - 5R_c) = \tfrac{1}{2}\times(5\cos\gamma_0 - 3)\times 100\%$$

and, for a refractive index of 1.5, we have $R = 36\%$.

If two photosensitive faces are viewed then the percentage of light collected now becomes $R' = 49\%$. It should be mentioned that this percentage of light could also be obtained with only one photosensitive face provided the opposite face is coated with a material having a reflection coefficient of one. In practice the reflection coefficient would always be less than one.

2-2.2 Design Considerations for Light Pipes

Light pipes operate on the principle that light entering within a critical angle γ_o, equal to the angle of total internal reflection, with the axis of the light pipe, will be transmitted along the light pipe with one hundred percent efficiency provided the cross-sectional area does not decrease [17]. Any decrease in the cross-sectional area will correspondingly give a decrease in the amount of light transmitted. In the case of light pipes which taper along their length while at the same time maintain constant cross-section it is necessary for the optimum transmission of light that the angle of taper is small. Light pipes which satisfy this condition are refered to as being adiabatic [17]. In practice when going from the rectangular face of a scintillator to the circular face of a photomultiplier the adiabatic condition is seldom satisfied. This is due to the difficulty in machining the exponentially tapered curve required to keep the cross-sectional area constant. Approximations to the adiabatic condition are made by constructing straight edge tapered light pipes. Alternatively, strip light pipes which twist along their length and are brought together at the photocathode can be used . The strip light pipes will remain adiabatic provided the angle of twist is small. The properties of the various light pipes have been investigated by several workers

2-9,17-23), and it has been found that the strip light pipes are the most efficient.

2-2.3 Absorption of Light in Scintillator and Light Pipes

Light absorption in the scintillator causes the light collection at the photocathode to be no longer independent of position at which the scintillation takes place. This is the main cause of the non-uniformity in large area scintillation counters.

The tedious calculation of the light arriving at the photocathode with the effect of the absorption included is not presented here since work [2,6] by others has shown that such calculations although giving the general trend of the non-uniformity do not agree sufficiently well with the experimental results. However, it is easy to visualize that two or more photosensitive faces will reduce the non-uniformity.

2-2.4 Reflection of Surfaces and Optical Contacts

In the case of large area scintillators where most of the light arriving at the photocathode has undergone multiple reflections, the most efficient surface for the walls is one which is totally internally reflecting. For small scintillators however, diffusely or specularly reflecting surfaces may be more efficient [24,25]. In both cases when only one photosensitive face is used the opposite face should be made diffusely or specularly reflecting. When diffusely or specularly reflecting surfaces are used the light collection will be dependent on the position at which the scintillation takes place.

The requirements of the material used to couple the scintillator to the light pipes and the light pipes to the photocathode are that the refractive index of the material is the same as that for the scintillator and light pipes and that the absorption of light is small at the wavelengths of interest.

2-2.5 Photocahtode Sensitivity

The counter uniformity is influenced by variations in the quantum efficiency from different positions on the photocathode. It is also affected , although to a lesser extent by the response of the photocathode to different wavelengths of light caused by the different absorption and reflection conditions in the scintillator and light pipes. The above effects are especially important in the case of the small counter where the scintillator has been placed directly onto the photocathode. The use of light pipes will eliminate this cause of non-uniformity by distributing the light across the entire face of the photocathode. They will however, decrease the collimated resolution of the counters by absorbing part of the light.

2-3 Design of Scintillator-Photomultiplier assemblies

2-3.1 Choice and Properties of Scintillators

The plastic scintillator NE-102 [26)] was chosen for its fast decay time, availability in relatively large sizes, suitability for connection to light pipes, and ease of handling. In the case of one of the large counters which was built later, the scintillator NE-110 with its better light absorption characteristics was used. Inorganic scintillators eg. sodium iodide with their better energy resolution were not chosen due to their slower decay time, their difficulty in handling, and the difficulty in manufacturing large sizes. Some of the properties of scintillator NE-102 are shown in Table 1.

When a particle is detected in the scintillator NE-102, light having a long wave and a short wave component is emitted. The short wave component is very easily reabsorbed and hence, in a graph of the light transmitted versus the distance from the light source [27], Figure 2, one sees an initial sharp drop in light followed by a slow decrease as the distance from the source is increased. It follows that, in the large counter this short wave component will be totally absorbed while in the small counter most of it will be collected provided the thickness of the small counter is just equal to the distance required to stop the incoming particles, which have energies up to 50 mev. From Figure 2 and the knowledge that the resolution of the counters are approximately inversely proportioal to the square root of the amount of light, L, collected by the phototube, one can expect that the ratio of the resolutions for the small and large counters is related as follows:

$$\frac{R_l}{R_s} = \sqrt{\frac{L_s \cdot Q_s \cdot G_s}{L_l \cdot Q_l \cdot G_l}}$$

Where, R_l and R_s represent the resolutions of the large and

TABLE 1

PROPERTIES OF SCINTILLATOR NE-102 [27]

Density (grams/cc)	1.032
Refractive Index	1.581
Softening Point (degrees centigrade)	75^{o}
Light Output (% Anthracene)	65%
Number of electrons per cc	3.4×10^{23}
Decay constant (seconds)	3×10^{-9}
Wavelength of maximum emission (angstroms)	4250
Ratio of number of carbon atoms to hydrogen atoms	1.105

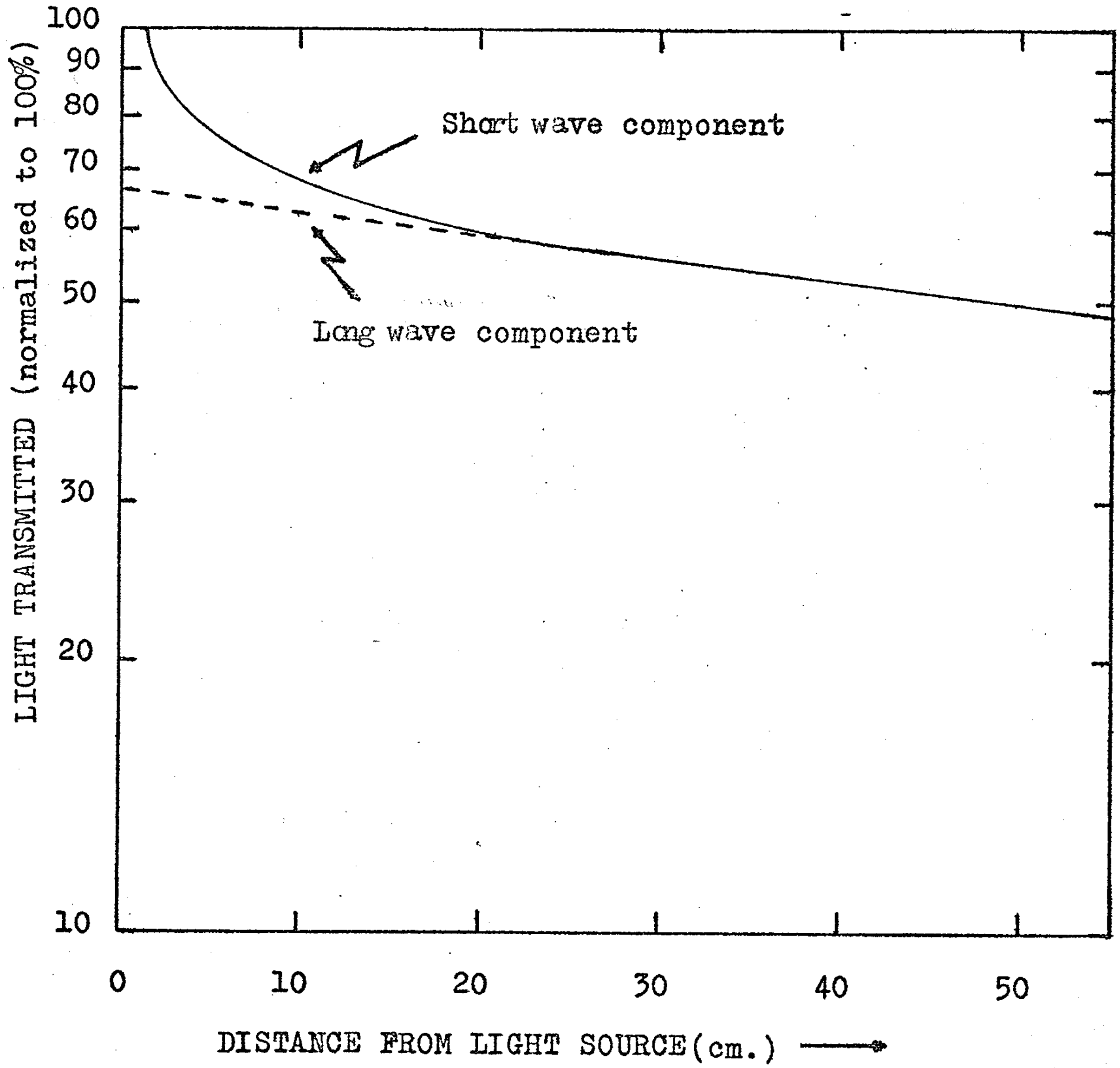

FIGURE 2

Absorption curve for the scintillation light in NE-102 scintillator.

small counters respectively. The resolution is defined as the full width at half maximum of the peak of monoenergetic particles entering the scintillator, divided by the energy of the particles. The quantum efficiency Q has been used in the calculations since the large and small scintillators are viewed by different phototubes. G_l and G_s have been incorporated as geometrical factors, to account for the different shapes of the large and small scintillators, and to a first approximation may be taken as unity. From Figure 2, L_s/L_l is approximately equal to 2.2, and from the data provided by the manufacturers of the phototubes Q_s/Q_l is of the order of 1.2. It should be pointed out that the ratio Q_s/Q_l was found from the ratio of the cathode sensitivities, which have been measured at a wavelength of one micron, and hence is used only as a first approximation in the above calculation which has assumed a spectral response of 4200 angstroms for the scintillators. Using the above numbers the ratio R_l/R_s becomes equal to 1.6. This value for the ratio of the resolutions can be taken as a lower limit to the expected value, since, in practice the geometrical factors which account for the different shapes and reflection conditions in the large and small scintillators will tend to increase it.

NE-102 has a non-linear response for protons below an energy of about 14mev [28] and this is shown in Figure 3. Since we are interested in protons with energies lying between 7 mev and 50 mev this effect is important. Fortunately it is pos-

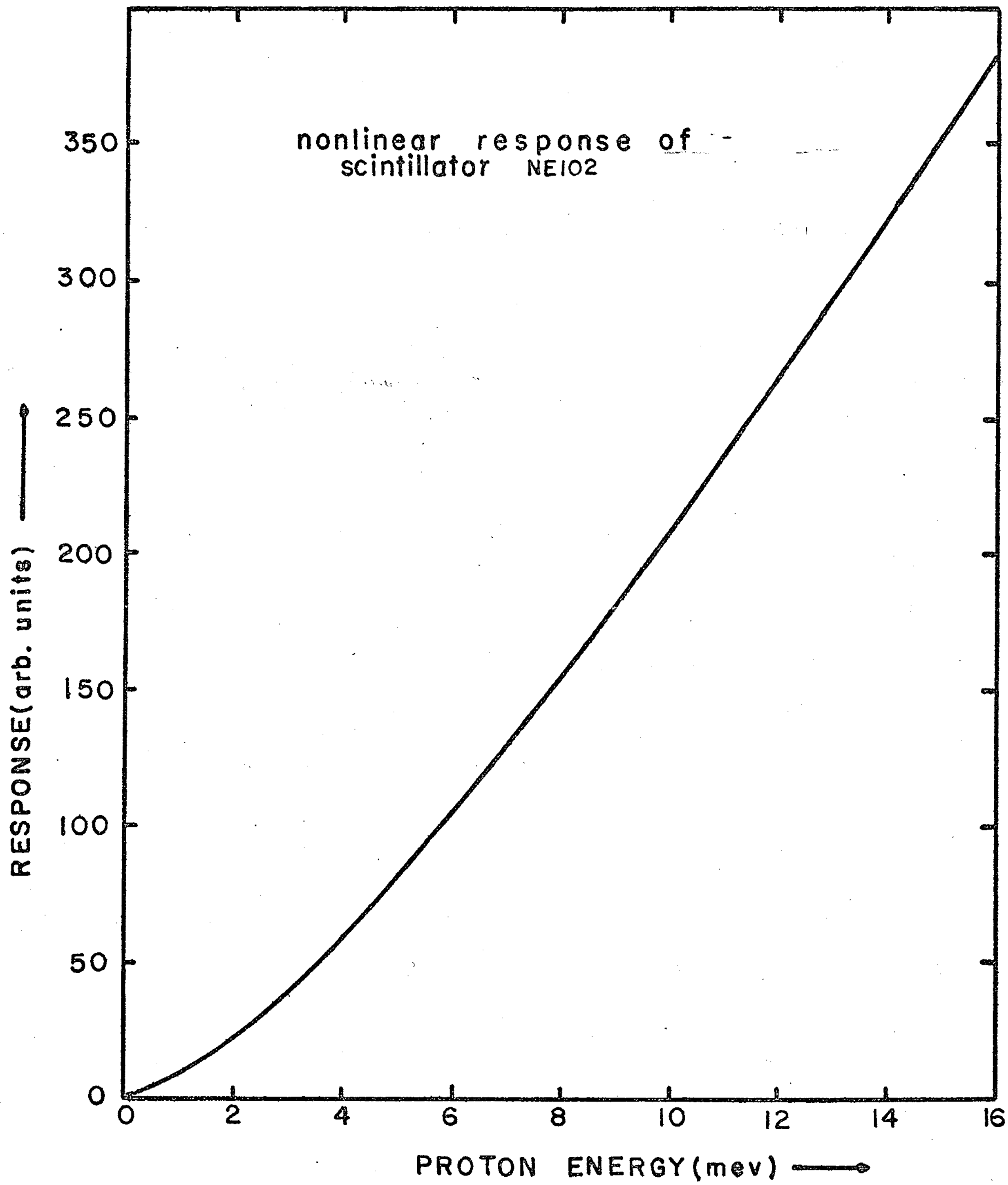

FIGURE 3

The response of NE-102 scintillator to low energy protons.

sible to correct to a certain extent for the non-linearity by using the space charge properties of the phototubes. Space charge effects, which are caused by high current densities in the phototube, also introduce a non-linearity, which is in an opposite sense to that described above, and hence, it is possible by careful adjustment of the phototube high voltage to diminish the non-linearity of the scintillator.

2-3.2 Design of Small Counters

The scintillator, 10.6 cm in diameter and 2.3 cm thick, is directly attached to a five inch phototube (EMI 9618R) using the potting compound RTV-615B [29]. In Figure 4 an exploded view of the small counter assembly is shown. An aluminium jacket (#4) is slipped over the scintillator and taped using black light tight tape to the phototube and mu-metal shield. An O-ring groove is cut in the front face of the jacket so that an aluminium foil, 1 mil thick (#8) forms a light tight fit when the brass ring (#9) and locking screws (#10) are in position. The O-ring #6 serves as a spacer. To ensure that the phototube was light tight it was painted with black non-conducting blackboard paint. The whole assembly was then wrapped with several layers of black tape. This arrangement enables the exchange of phototube base circuits by simply removing the inner mu-metal shield (#2) which they are attached to without disturbing the mounting of the scintillator.

The potting compound was used rather than the conventional methods [30], eg Dow Corning 200 Fluid, since a material intermediate between cement and fluid was required

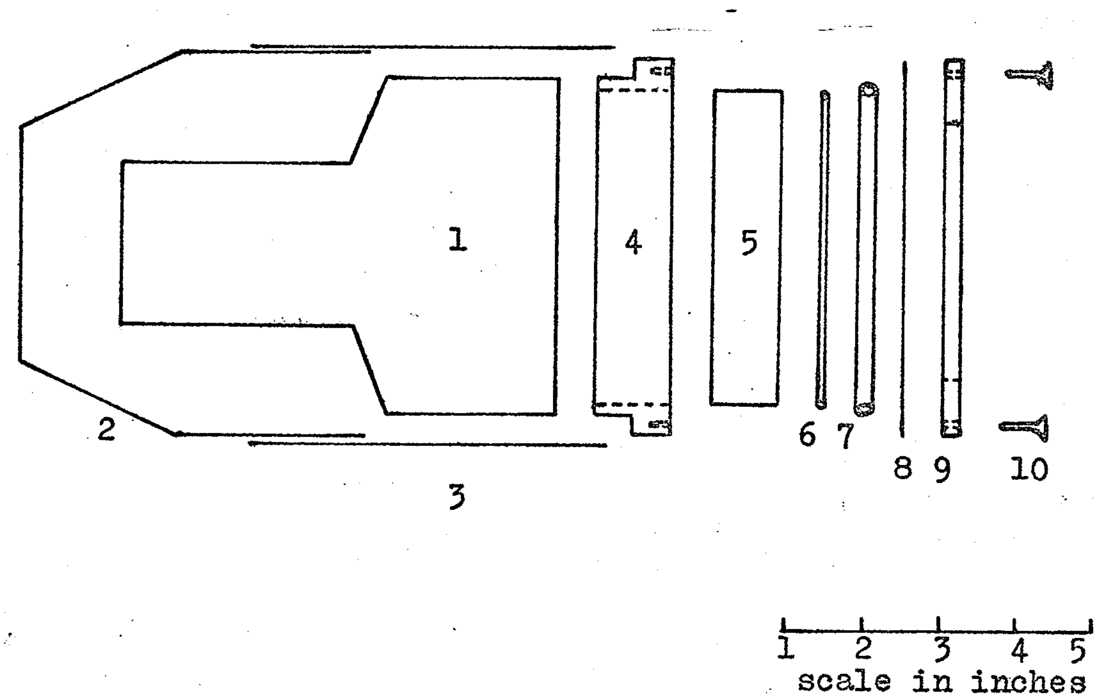

FIGURE 4

Exploded view of small counter assembly, where 1 - EMI 9618R phototube, 2 - Inner mu-metal shield, 3 - Outer mu-metal shield, 4 - Aluminium ring assembly (connected to phototube and outer mu-metal shield with black tape), 5 - Scintillator NE-102, 6 - O-ring spacer, 7 - O-ring, 8 - Aluminium foil, 9 - brass ring (determines the effective area of the scintillator), and 10 - locking screws.

in order that the base circuit could be changed without seriously disturbing the optical contact. No precise tests were performed on the potting compound prior to its use with the counter, however, it was found to give similar results for the energy resolution as to that given when the Dow Corning 200 Fluid was used.

2-3.3 Design of Large Counters

Two rectangular scintillators 22.5×22.5×2.5 cm^3 coupled to strip light pipes 30 cm long on two opposing faces have been built. The first scintillator-light pipe assembly consisting of the scintillator NE-102 coupled to polyvinyltoluene light pipes was manufactured by Nuclear Enterprises Ltd., while the second, made from NE-110 scintillator and lucite light pipes was constructed by our own workshop. In the latter case the scintillator was joined to the light pipes with NE-580 optical cement. Figure 5 is a photograph of the large counter assembly and in Figure 6 an exploded view of the mounting arrangement used is shown. The scintillator and light pipes are surrounded by an opaque acrylic cover (#9) made by heating 1/16 inch thick acrylic sheet with a bunsen flame and bending, when soft, over a mould similar in shape to that of the scintillator and light pipes. The mould itself was made from wooden strips, one inch thick plywood, with the space between the strips filled in with plaster. The cover, which is in five parts, is designed such that there is at least a half inch space between it and the scintillator and light pipes. In one of the counters the

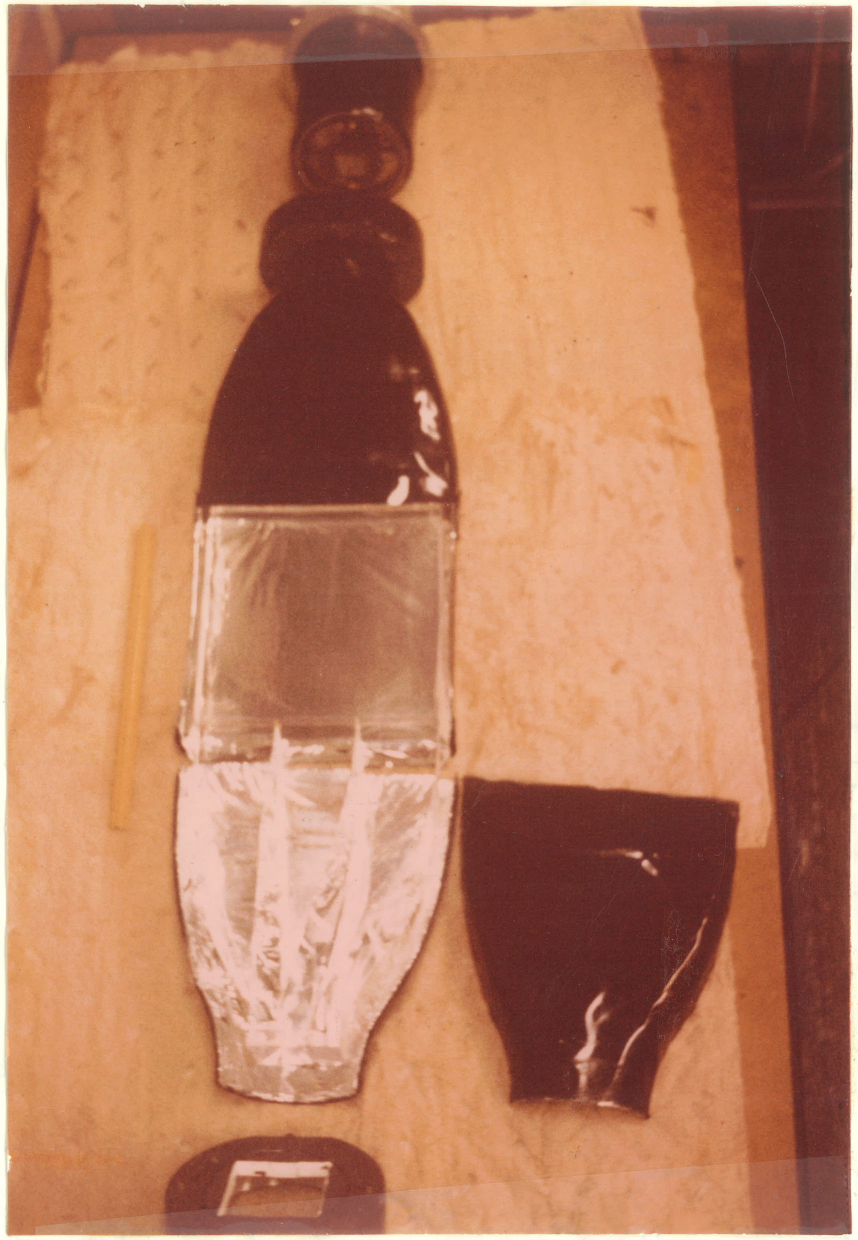

FIGURE 5

Photograph of large counter assembly

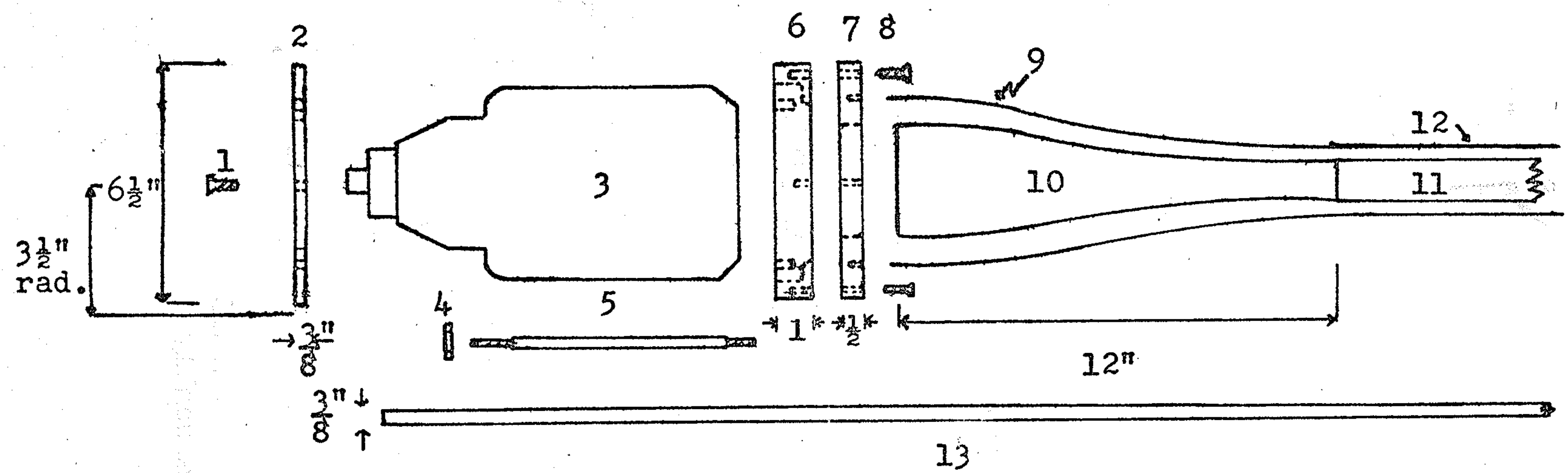

FIGURE 6

Exploded view of large counter assembly, where:

1 - 3×120° screws(provided by the phototube manufacturers) which attach the aluminium disc(2) to the rear of the phototube. 2 - 3/8" thick aluminium disc, 7" outside dia. with $\frac{1}{4}$" facets at top and bottom. 3 - XP1040 phototube. 4 and 5 - four sets of nuts and long screws which attach the disc(2) (and hence the phototube) to the coupling(6). 6 - 1" thick Al. coupling rings. 7 - $\frac{1}{2}$" thick opaque acrylic disc with centre part cut such that it fits tightly onto end of light pipe(10), $\frac{1}{4}$" groove cut in one of the faces to accommodate the acrylic cover (9). 8 - 4×90° screws which attach (6) to (7) 9 - opaque 1/16 in. thick acrylic cover. 10 - light pipes 11 - scintillator. 12 - Al. foil. 13 - Base plate.

inside of the cover is lined with specularly reflecting aluminized mylar foil held in place by double sided Scotch tape, while in the other NE-560 diffusely reflecting paint has been used. The cutting and finishing of the acrylic cover was accomplished by using a small portable hand drill fitted with thin circular grind stones. An entrance window consisting of 1 mil thick aluminium foil allows protons to enter the scintillator (#12). The scintillator-light pipe assembly along with the acrylic cover is attached to a base plate by means of two opaque acrylic discs (#7) whose centre parts have been cut such that they fit onto the ends of the light pipes tightly so that no gluing is necessary. Attached to the discs are aluminium rings (#6) designed to fit over the front of the phototubes. The phototube can be brought up to the light pipes by means of four long screws (#5) which run from the aluminium ring at the front of the phototube to aluminium discs (#2) attached to the rear of the phototube (by means of the three screw holes in the mu-metal shield provided by the manufacturers). When the potting compound, which joins the light pipes to the photocathode,has set,the assembly is locked in place by means of screws attached to the base plate (#13).The joints in the assembly were made light-tight with the use of putty and black tape. Finally the base plate was attached to an adjustable stand and placed behind the wire chambers. This arrangement enabled the scintillators to come within two inches of the wire chambers.

CHAPTER III

PHOTOMULTIPLIERS AND BASE CIRCUITS

3-1 Choice of Photomultipliers

In the case of the small counters, photomultipliers having good quantum efficiency, small photocathode non-uniformities, and relatively fast rise and transit times were required. The EMI 9618R phototubes, selected at the factory for photocathode non-uniformities less than 10%, satisfied these conditions.

In the case of the large counters where the photocathode non-uniformity is not so critical, since the light from any point in the scintillator is distributed across the entire face of the photocathode, the emphasis has been placed on the rise and transit times of the phototube. The Philips XP1040 phototubes with rise times of 2 nano seconds and transit times of 45 nano seconds were chosen to view the large scintillators*.

Table 2 shows some of the properties of the EMI 9618R and Philips XP1040 phototubes.

3-2 High Voltage Power Supply

To eliminate the need for high voltage coupling capacitors which may introduce noise, negative high voltage was used. This required the phototube to be insulated from the mu-metal shield to ensure that no electrical breakdown would

* The RCAC70133B phototubes having higher photocathode efficiency would have been preferable, however it was judged that the improvement in performance would not justify the higher price.

TABLE 2

PROPERTIES OF PHOTOMULTIPLIERS USED†

Photomultiplier	EMI 9618R	Philips XP1040
Photocathode material	Cs_3Sb-O	Cs-Sb
Spectral response curve	S-11	A(S11)
Wavelength at maximum response	4100Å	4200±300Å
Luminous Sensitivity *	85	70
Maximum useful diameter	111 mm	110 mm
Multiplication stages	11	14
Dynode type	Venitian Blind	Linear Focussed
Dynode material	CsSb	AgMgO-Cs
Rise time	10 ns	2 ns
Transit time		45 ns

† Abstracted from the manufacturers manuals [33,34)]

* Average of four phototubes which we have bought from the manufacturers.

occur. By wrapping several layers of black insulation tape around the photomultipliers we were able to solve this problem.

In the case of the large counters the two photomultipliers which view the top and bottom sides of each scintillator were, due to economy, driven by the same power supply. This was achieved by passing the output of the power supply through a distribution box consisting of an input and two outputs. Since it was necessary to match the gains of the phototubes accurately, one of the outputs was kept at the voltage of the input, while in the other the voltage could be varied by means of a potentiometer connected in series with the input. In the later case a resistor was placed in series with the potentiometer, the value of which depended on the difference in operating voltages of the two phototubes. This arrangement enabled the gains of the phototubes to be matched to one or two percent in a 1024 channel ADC.

3-3 Properties of the Dynode Chain

The simplest form of base circuit is the linear resistor chain where the value of all resistors between dynodes are equal. This base circuit is normally sufficient to provide the high gain necessary for most applications, however, in certain cases where the maximum gain is desirable each individual resistor should be adjusted until the optimum operating condition is attained. Another type of resistor divider chain is employed when the density of the electron current in the phototube becomes so large that space charge effects become apparent at the last stages. This resistor chain has the value of the resistors at the last stages increasing according to a three halves law. The dynodes in this case have been assumed to operate in a similar manner to that of a simple diode valve, where the effects of space charges are relatively well known.

The circuit between photocathode and first dynode is different for different phototubes due to the various focussing and accelerating electrodes. The voltage on these electrodes may be adjusted to satisfy one or more of the following conditions:

1) Maximum pulseheight.
2) Maximum energy and/or time resolution.
3) Minimum transit time.
4) Minimum photocathode non-uniformity.

It has been shown [31] that for the optimum performance of the Philips XP1040 phototube the voltage of the focussing electrodes should be carefully set.

The situation at the final stages is slightly different. Under normal operating conditions the signal current is superimposed on the chain current and the response of the tube becomes non-linear [32]. To understand this effect it is convenient to first consider the situation when the tube is in continuous operation i.e. the d.c. mode. The signal current at the last stages will cause the voltage across these stages to decrease and since the overall voltage on the phototube remains constant these decreases may be regarded as voltage increases on the earlier stages and the gain of the tube will be increased. Different signals will be associated with different gains, and consequently this will introduce the non-linearity. With a chain current one hundred times the signal current the non-linearity will be of the order of one percent. When the photo-tube is operating in the pulsed mode, the stage voltages will follow the variation in the instantaneous signal current and the gain of the tube will be altered correspondingly giving distortion to the input signal. If, however, capacitors are connected across the last stage resistors such that the individual time constants are much greater than the period of the pulse, then the dynode voltages at the last stages will be stabilized against variations in the instantaneous signal current. The value of the last decoupling capacitor is given by;

$$C_1 = \left(\frac{I_a \times t}{V} \times 100 \right) \times 10$$

where, I_a equals the maximum <u>average</u> signal current , t equals the length of the longest pulse, and V equals the voltage across the last stage. The factor of one hundred makes sure that the variation is less than one percent, and the factor of ten arises from the fact that the change in gain is approximately ten times the change in voltage. The value of the other decoupling capacitors can be decreased from the anode downwards according to the relations;

$$C_2 = 1/g \times C_1 \ , \quad C_3 = 1/g \times C_2 \ , \quad \text{etc.}$$

where, g equals the stage gain for the dynodes. The gain of the tube will now remain approximately constant for the duration of the pulse at a value determined by the average d.c. level of the signal current. If, however the amplitude of the signal, or the counting rate changes, then the average signal current will also change and the gain of the tube will be altered. If the chain current is made large enough or the last stage resistors replaced by voltage stabilizers such as zener diodes the above effects can be reduced to negligible proportions. It should be pointed out that even although ample precaution has been taken to minimize the loading effect described above, the tube may still be count rate dependent due to a property of the dynodes themselves.

3-4 Space Charge Effects in the Photomultiplier

Space charge effects at the last dynode stages cause the large pulses to become saturated, and hence, another type of non-linearity is introduced. This time the non-linearity is in an opposite sense to the non-linearities described before. The effect depends on the charge density of the electrons, which in turn depends on the amount of light reaching the photocathode, the dynode number, the type of base circuit used, and the overall voltage on the phototube. Since the effect is similar to the space charge effects in an ordinary diode valve, increasing the value of the resistors towards the anode according to a three halves law should reduce the effect. As a consequence of the space charges it is possible by raising the overall voltage on the phototube to produce pulses that are slightly saturated at the anode of the photomultiplier, and progressively become linear as the dynode stages are decreased towards the photocathode.

3-5 Output Pulses from the Photomultiplier

As mentioned before in the introduction, two pulses are required from each photomultiplier; (1) a fast timing pulse taken from the anode, and (2) a linear analog pulse taken from one of the dynodes. The dynode pulses are taken through a 50 ohm load resistor, which goes to earth via the decoupling capacitors, and into a coupling capacitor which eliminates the d.c. high voltage. The positive dynode pulses are then inverted by a pulse transformer (EG&G IT100) and sent via 50 ohm double shielded cable to the control room.

In the case of the large counters where two phototubes are used to view each scintillator the pulses from both tubes are added together in mixer modules (EG&G AN102/N). The mixed dynode pulses are sent to the control room where they are stretched and digitized. The anode pulses are also mixed and used to select the events of interest and to trigger the wire chambers.

CHAPTER IV

TESTING OF PHOTOMULTIPLIERS AND BASE CIRCUITS

Since the photomultipliers were required to operate with very high signal currents, due to the large amplitude and high counting rate of the pulses, it was necessary to do some extensive testing to decide which base circuit was the most suitable, which dynode to choose for an energy measurement, and the approximate overall operating voltage.

4-1 Method Used to Test Linearity of Photomultipliers

To test the linearity of the scintillators and phototubes, protons were scattered from a polyethelene (CH_2) target, 6 mils thick, and observed at the center of the scintillators at an angle of 45^o. The pulseheights of the elastically scattered protons from the carbon and hydrogen nuclei were then observed on an oscilloscope. Theoretically, from the kinematics of elastic scattering, the pulseheights should be in a ratio of 1.9 to 1. However, due to the unequal energy losses in the materials subsequent to the arrival of the particles at the scintillators, this ratio will be increased to approximately two to one. The non-linear response of the scintillator will increase the carbon to hydrogen pulseheight ratio while the space charge effects will tend to decrease it. The effect of the space charge saturation on the pulseheights can be studied by measuring the height of the carbon and hydrogen pulses for various overall phototube voltages. By observing the pulseheights from the anode and various dynodes of each phototube and plotting the log of the pulseheight against the phototube voltage we were able to determine which dynode was the most suitable for our application. Since the height of the dynode pulses should be large compared to the noise in the transmission lines (ie radio frequency pick-up from the cyclotron) the above measurements were repeated, in the case of the EMI phototubes, using different base circuits in an effort to determine which base circuit gave the largest linear dynode pulses.

4-2 Base Circuits and Results for the EMI 9618R Photomultipliers

The base circuit that was first tried for the EMI 9618R phototube was the one recommended by the manufacturers for high gain and high current [33]. However, it was soon discovered that the non-linearity due to space charge effects appeared before the required pulseheights were reached. Reducing the voltage on the phototube had the effect of increasing the rise time of the anode pulse from 12 ns to around 17 ns and hence decreased the timing resolution in the spectrometer. It was also necessary to amplify the pulses. Part of the problem arose from the fact that after the overall tube voltage was reduced the voltage across the resistor between the photocathode and first dynode was approximately half that recomended by the manufacturers. This was solved by replacing the resistor by a series of zener diodes. The pulseheights, however, still remained low.

Figure 7 shows a test circuit that was built in order to

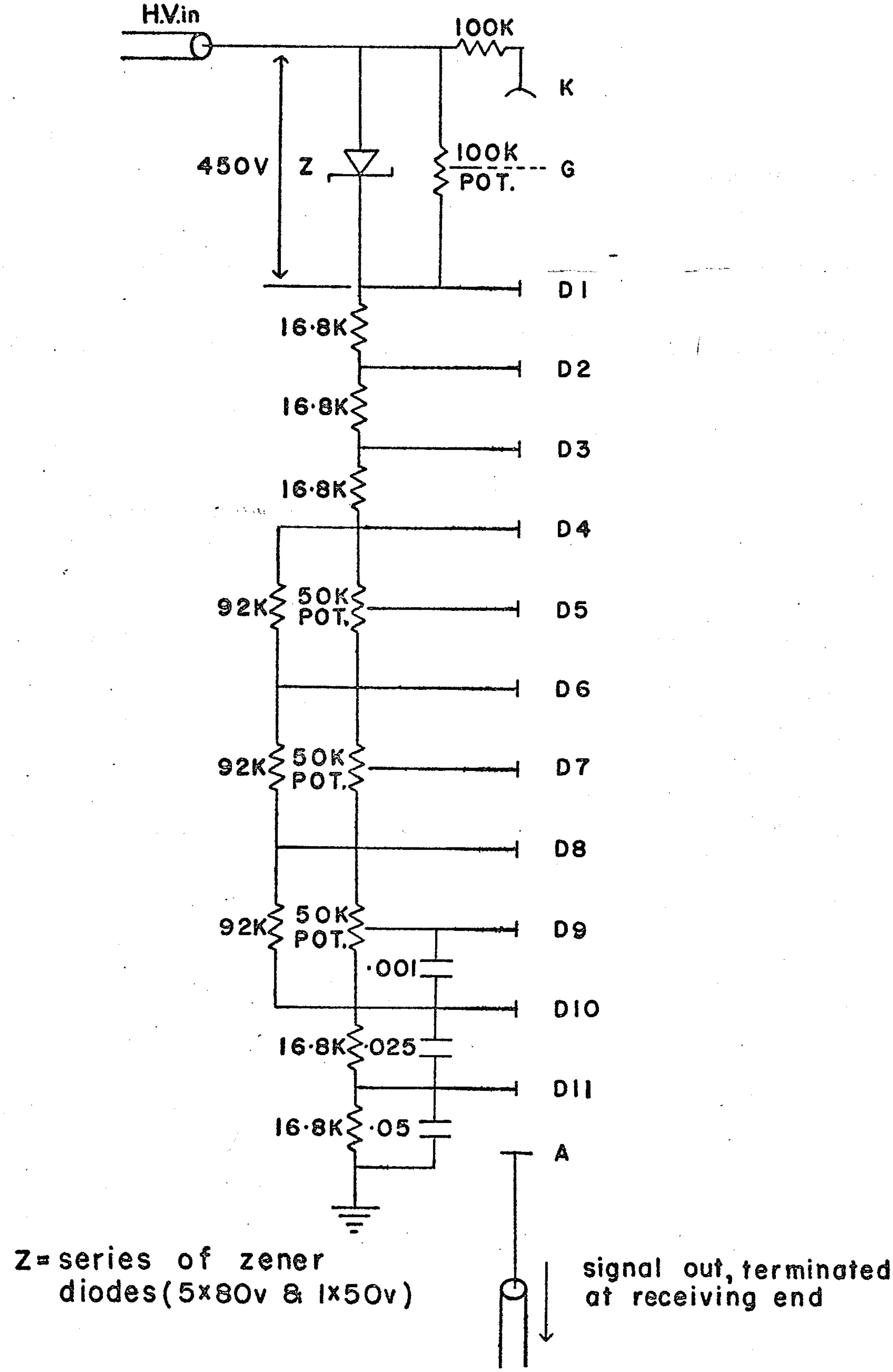

FIGURE 7

Test circuit for EMI 9618R

investigate the possibility of using a non-linear base circuit to reduce the effect of space charge saturation. It was hoped that by increasing or decreasing the voltage on alternate dynode stages that some defocussing of the electrons would take place which would decrease their charge density and hence reduce the space charge saturation. It should be pointed out that a base circuit in which the last stage resistors were increased according to a three halves law was tried, and found to give little improvement over the recommended one described above. The zeners between photocathode and first dynode, in Figure 7, have been shunted by a 100 kilo-ohm potentiometer in order that the effect of the focussing electrode could be studied. Figure 8 shows the results when the voltage on the focussing electrode is varied between that of the cathode and that of the first dynode. In these measurements the rest of the potentiometers were set such that the linear base circuit of 16.8 kilo-ohm was obtained. By varying the 50 kilo-ohm potentiometers between dynodes, 4 and 6, 6 and 8, and, 8 and 10 the voltages on dynodes 5,7 and 9 were changed to form several non-linear base circuits. For each circuit tried the carbon to hydrogen pulseheight ratio for the anode was measured for various overall phototube voltages. In order to find which base circuit gave the largest linear pulses, the carbon to hydrogen pulseheight ratio was plotted against the height of the hydrogen pulse, Figure 9. The curves of Figure 9 clearly show that base circuits in which the voltages on alternate dynodes are changed can give better results for the linearity at a particular pulseheight than the linear or near linear base circuits.

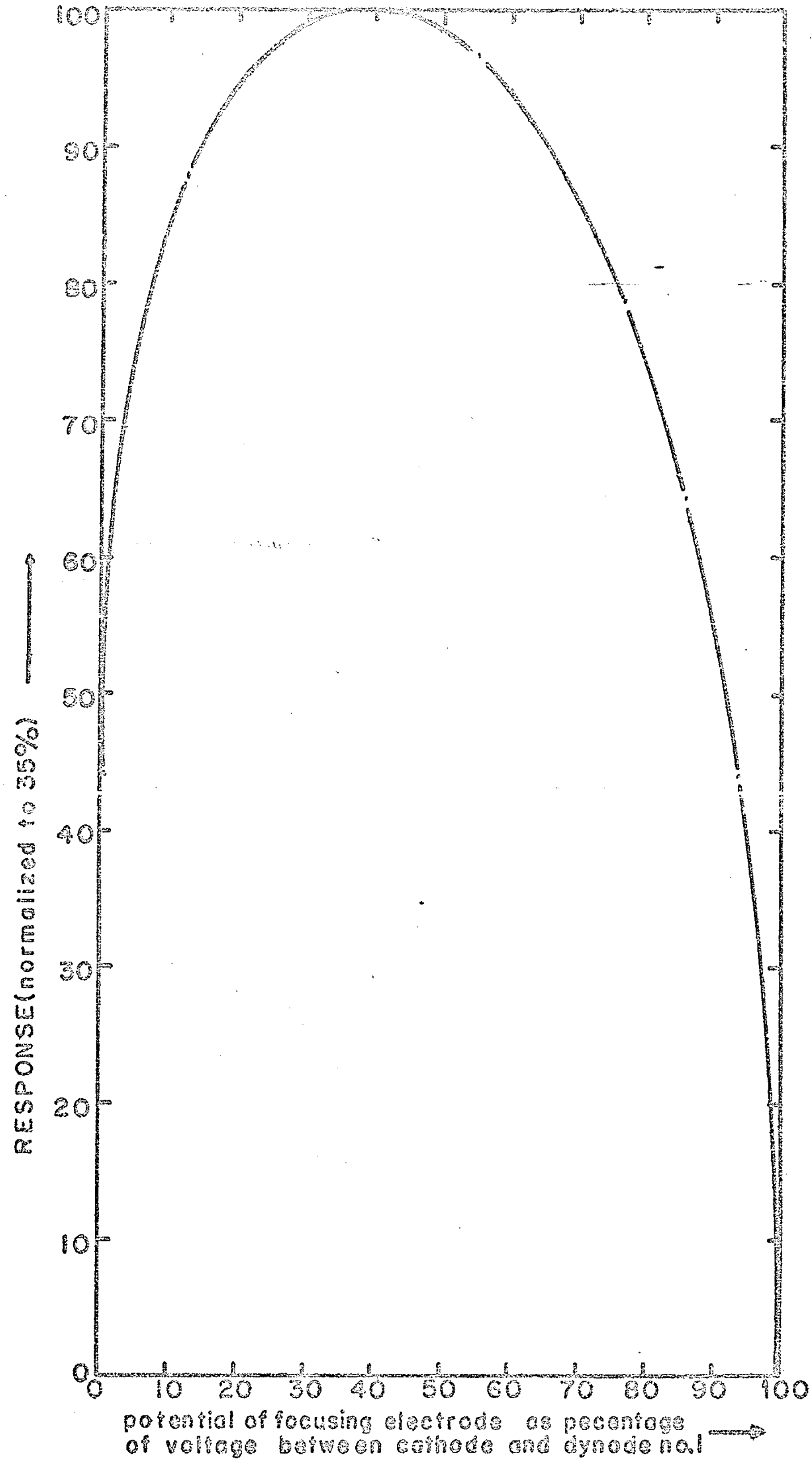

FIGURE 8

THE EFFECT ON THE RESPONSE OF THE EMI 9618 PHOTOTUBE AS THE FOCUSING ELECTRODE IS VARIED IN POTENTIAL.

Figure 9

Carbon to hydrogen pulseheight ratio plotted as a function of the hydrogen pulseheight for the small counter.

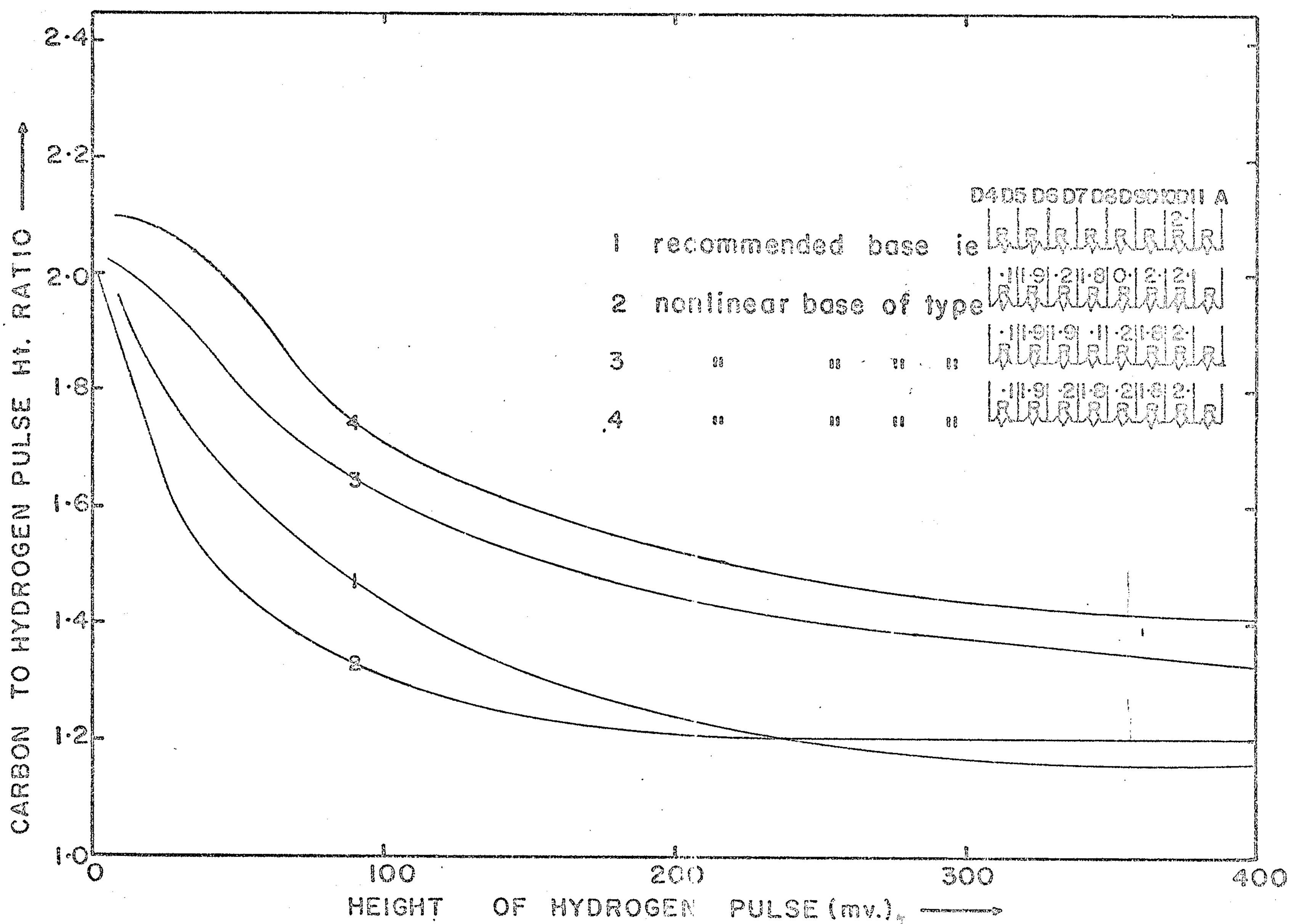

CARBON TO HYDROGEN PULSE Ht. RATIO
HEIGHT OF HYDROGEN PULSE (mv.)
1 recommended base ie
2 nonlinear base of type
3 " " " "
4 " " " "
D4 D5 D6 D7 D8 D9 D10 D11 A
2·4
2·2
2·0
1·8
1·6
1·4
1·2
1·0
0
100
200
300
400

From the considerations of the above, the base circuit shown in Figure 10 was constructed. Here the resistors between dynodes 2 and 3, 4 and 5, and, 6 and 7 are one tenth the value of the resistors in the preceeding stages, and the resistors at the last stages have been increased. The final resistor between dynode number 11 and the anode was not increased, in accordance with the manufacturers statement that any increase in this resistor will not seriously affect the space charge saturation. An output from dynode 10 is shown in the figure, however in order to investigate the effects in the other dynode stages outputs from dynodes 7, 8, 9, and 11 were also taken. The dynode pulses for the carbon and hydrogen protons scattered from the CH_2 target at 45^o were inverted and sent to the control room, via 250 ft doubly shielded cables, where they were observed on the oscilloscope. The log of the pulseheights plotted against the overall voltage on the phototube for some of the dynodes and for the anode are shown in Figure 11. From the graphs the effect of the space charge saturation is seen in the change of slope of the lines between 1300 and 1600 volts. The pulseheights from dynodes below dynode number eleven are very small. The reason for this is shown in Figure 12 where the shapes of the pulses from dynode 7 to the anode are reproduced from photographs taken of the oscilloscope traces. Here the phototube has been operated at an overall voltage of 1800 volts and the pulseheights have been multiplied by a factor of 1.54 to correct for the attenuation in the cable. Below dynode 11 long tails appear in the dynode pulses which are not accountable for from the considerations of space charges alone and are probably due to the design of the base

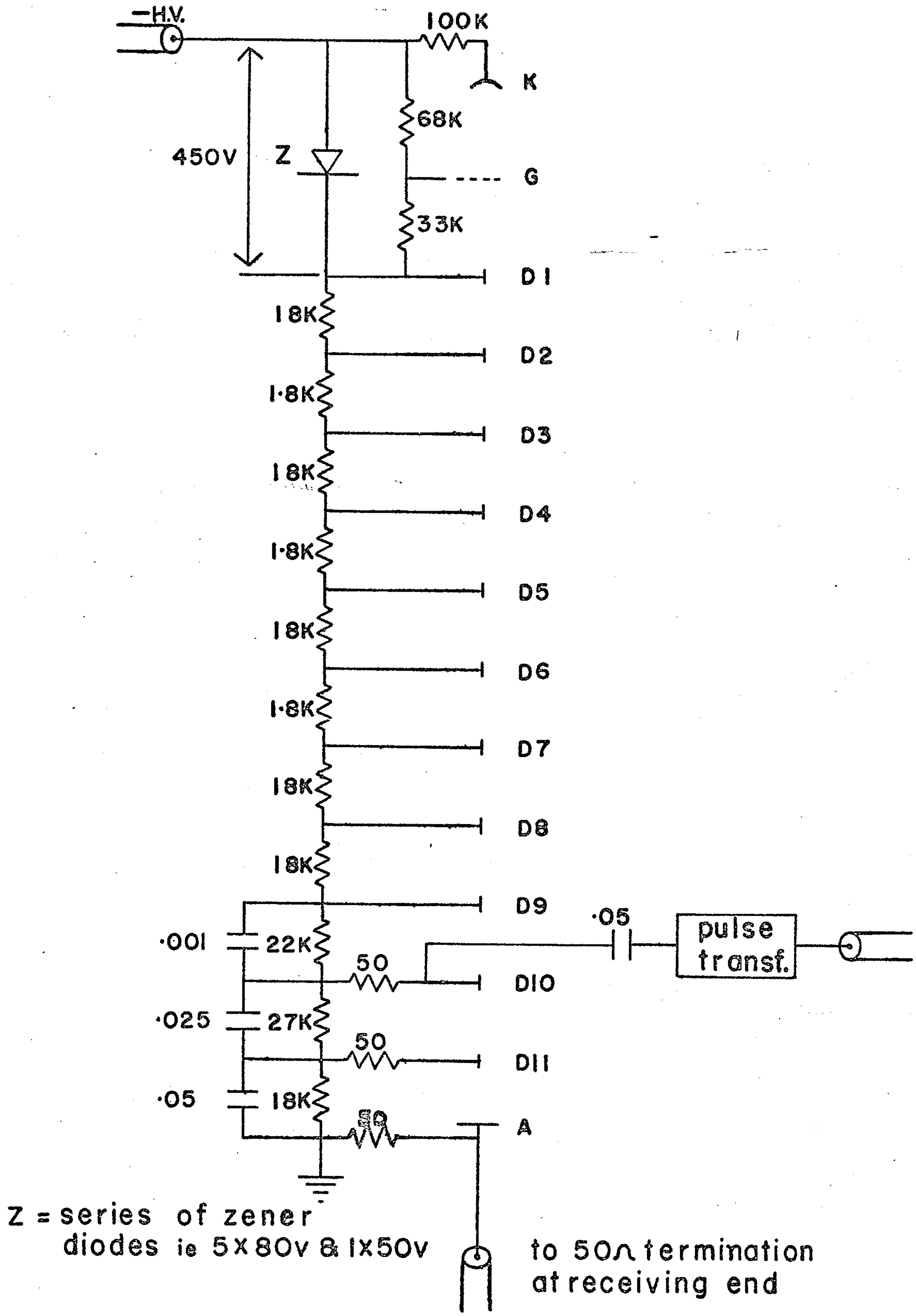

FIGURE 10

Base circuit for EMI 9618R

Figure 11

Pulseheight versus overall phototube voltage for protons scattered from a CH_2 target at 45° for one of the EMI 9618R phototubes. The pulseheights were measured on an oscilloscope 250 feet from the phototube.

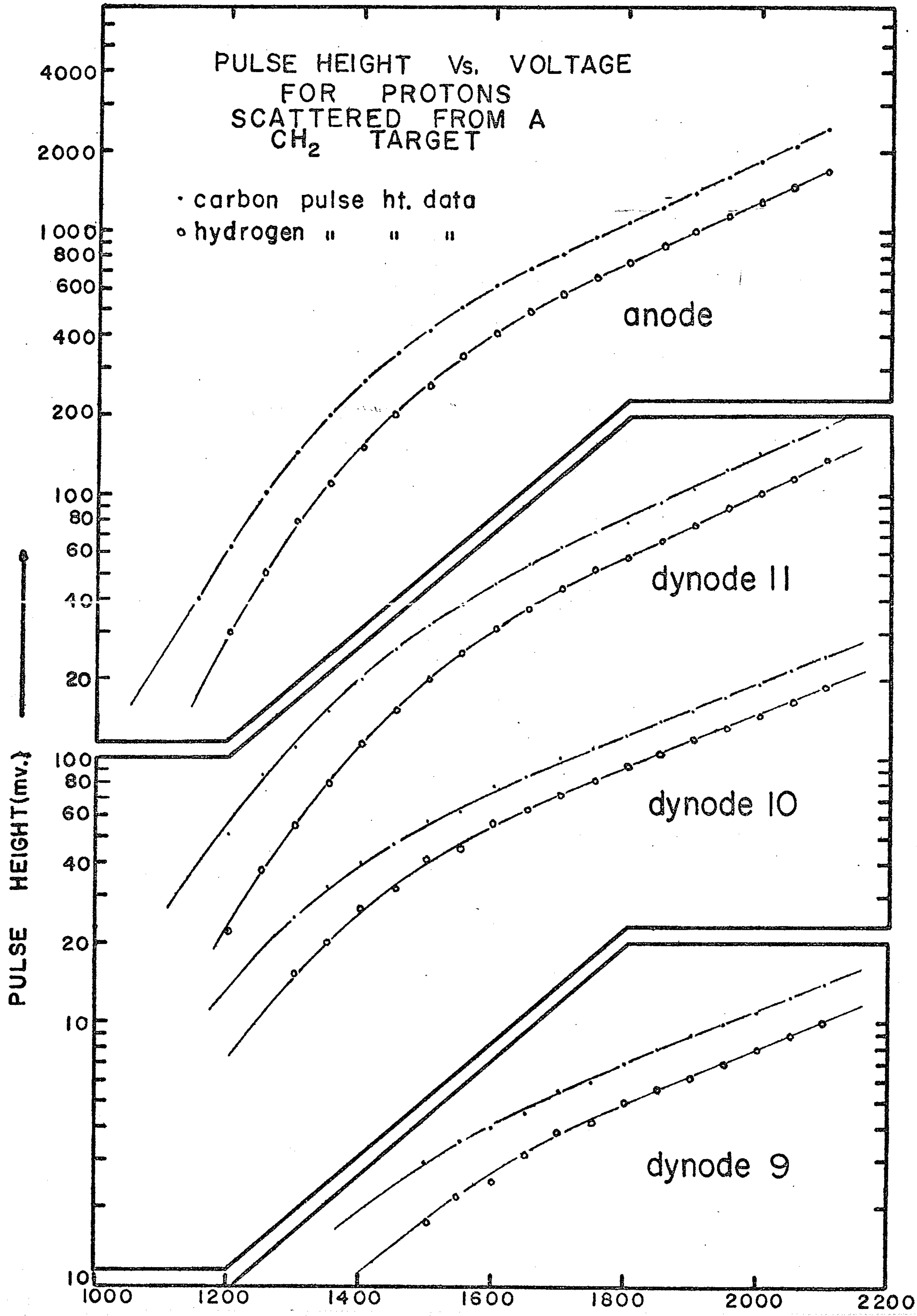

PULSE HEIGHT Vs. VOLTAGE
FOR PROTONS
SCATTERED FROM A
CH2 TARGET
· carbon pulse ht. data
o hydrogen " " "
anode
dynode 11
dynode 10
dynode 9
PULSE HEIGHT (mv.)
4000
2000
1000
800
600
400
200
100
80
60
40
20
10
1000
1200
1400
1600
1800
2000
2200

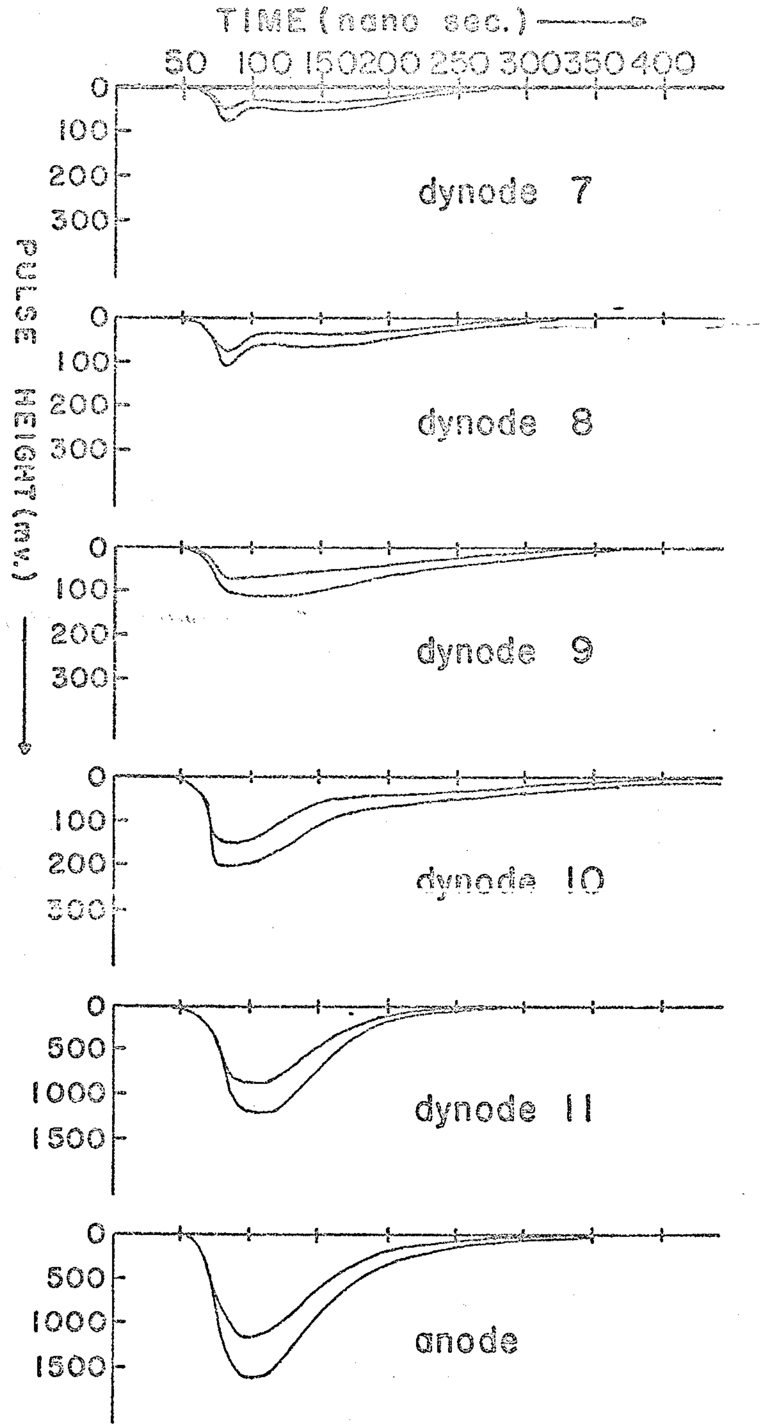

FIGURE 12

Pulse shapes from EMI 9618R

circuit.

The base circuit of Figure 10 was used in some preliminary tests of the spectrometer with the analog pulse taken from dynode number 11, however, it is obvious from the shapes of the pulses as seen in Figure 12 that more work is necessary before the base circuit most suitable for our application is obtained. Due to the time available and the fact that the large counters proved to operate satisfactory these further studies have still to be undertaken. Using the base circuit of Figure 10, under normal operating conditions average currents of around .4 ma were obtained with count rates of 10^5/sec.

4-3 Base Circuits and Results for the Philips XP1040 Photomultipliers

The base circuit used with the XP1040 phototubes is shown in Figure 13. It is essentially the linear resistor chain recommended by the manufacturers [34], except here the last four resistors have been replaced by zener diodes. The reason for the zeners is to reduce the effect of the larger pulseheight non-linearity caused by the higher count rates in the large counters. With the introduction of zeners into the divider chain it was found that the pulses from dynodes 10 and 11 were badly distorted by ringing with a period of about 10 ns. The problem was solved by replacing the last decoupling capacitor with a larger one, and inserting a 33 ohm resistor in series with it. A 10 ohm resistor was also inserted at dynode 12 to dampen the ringing, however its effectiveness was small compared to the solution described above.

Again extra dynode outputs were taken to observe the

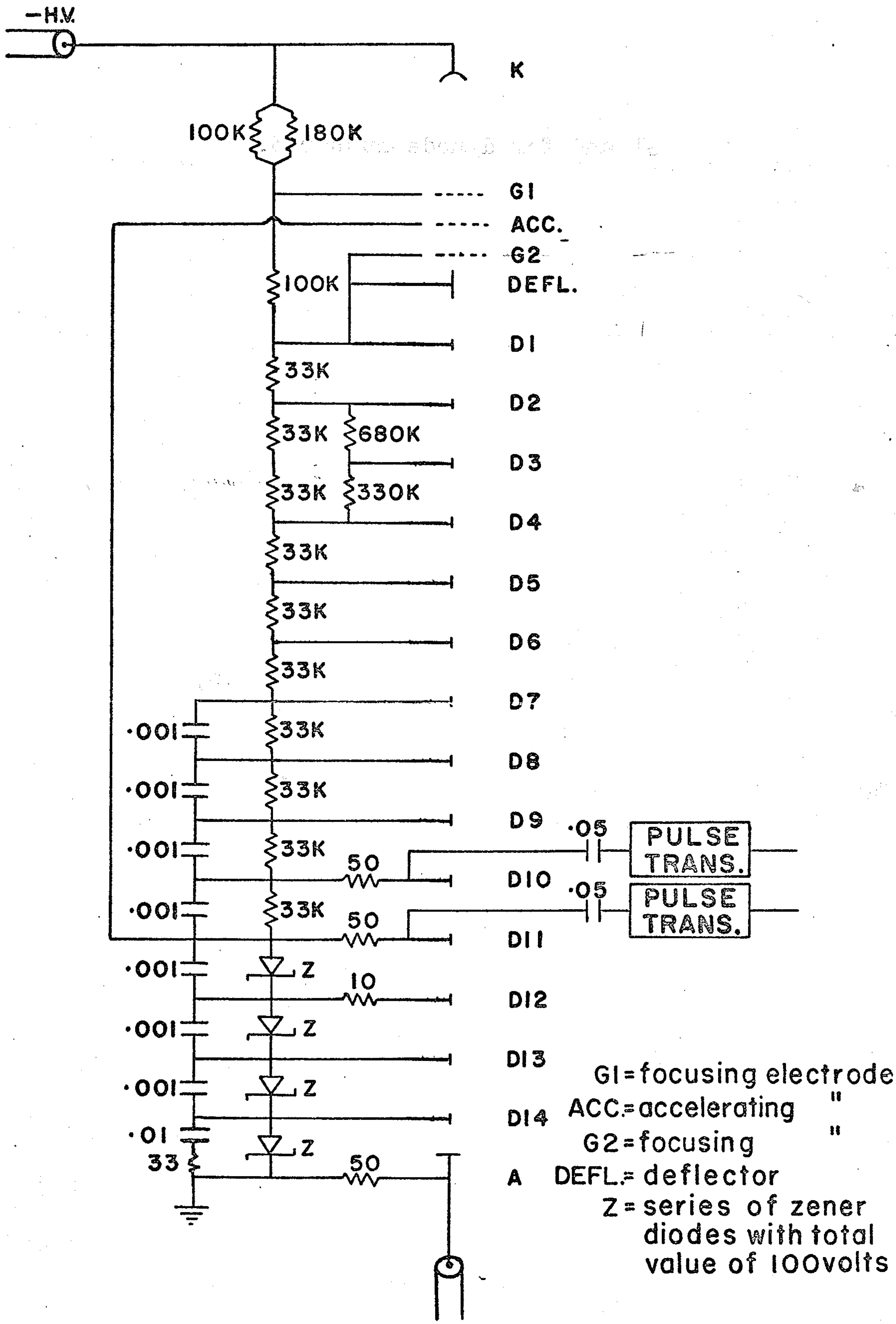

FIGURE 13

Base circuit for XP1040

effects of space charge saturation, and potentiometers were inserted to find the optimum voltage for the focussing electrode G1 and for dynode number 3.

Using a gamma ray source (Co^{60}) the voltage on the focussing electrode, G1 was adjusted until the maximum anode pulseheight was observed on an oscilloscope. It was found however, that the response of the tube varied rather sharply when the voltage on dynode number 3 was varied, between that of dynodes 2 and 4, and it was decided to adjust the voltage under normal operating conditions. The results are shown in Figure 14, where the pulseheights from the anode have been normalized to one hundred percent at the optimum voltage of the dynode. It was also found that the position of the peak in Figure 14 did not change as the overall voltage on the phototube was increased or decreased.

Figure 15 shows the variation of pulseheights from dynodes 11 to 14 and the anode, for the base circuit of Figure 13 (modified for dynode outputs) as the overall voltage on the phototube is increased. In this case, as before, protons were scattered from a CH_2 target and the scattered protons from the hydrogen and carbon nuclei at 45° were observed on an oscilloscope in the control room.

Figure 16 shows the shapes of the pulses from dynodes 10 to 14 and the anode at an overall phototube voltage of 1800 volts. Here the possible effects of space charge saturation are seen in the height and length of the pulses. The pulseheights have been multiplied by a factor of 1.25 in this figure to account for the attenuation in the cable (we used a

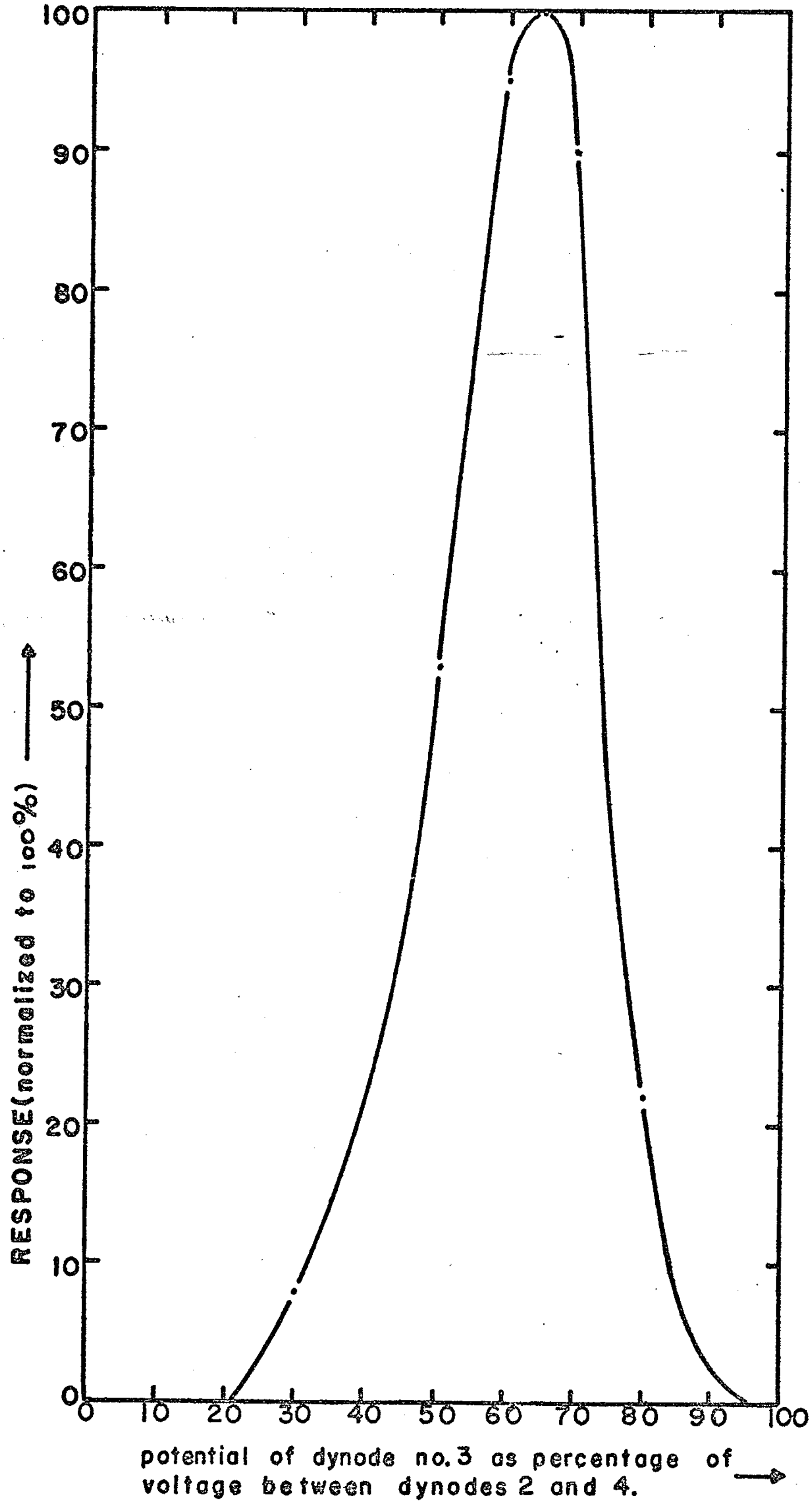

FIGURE 14

The effect on the response of the XP1040

phototube as dynode no. 3 is varied in potential

Figure 15

Pulseheight versus overall phototube voltage for protons scattered from a CH_2 target at 45^{o} for one of the Philips XP1040 phototubes. The pulseheights were measured on an oscilloscope 250 feet from the phototube.

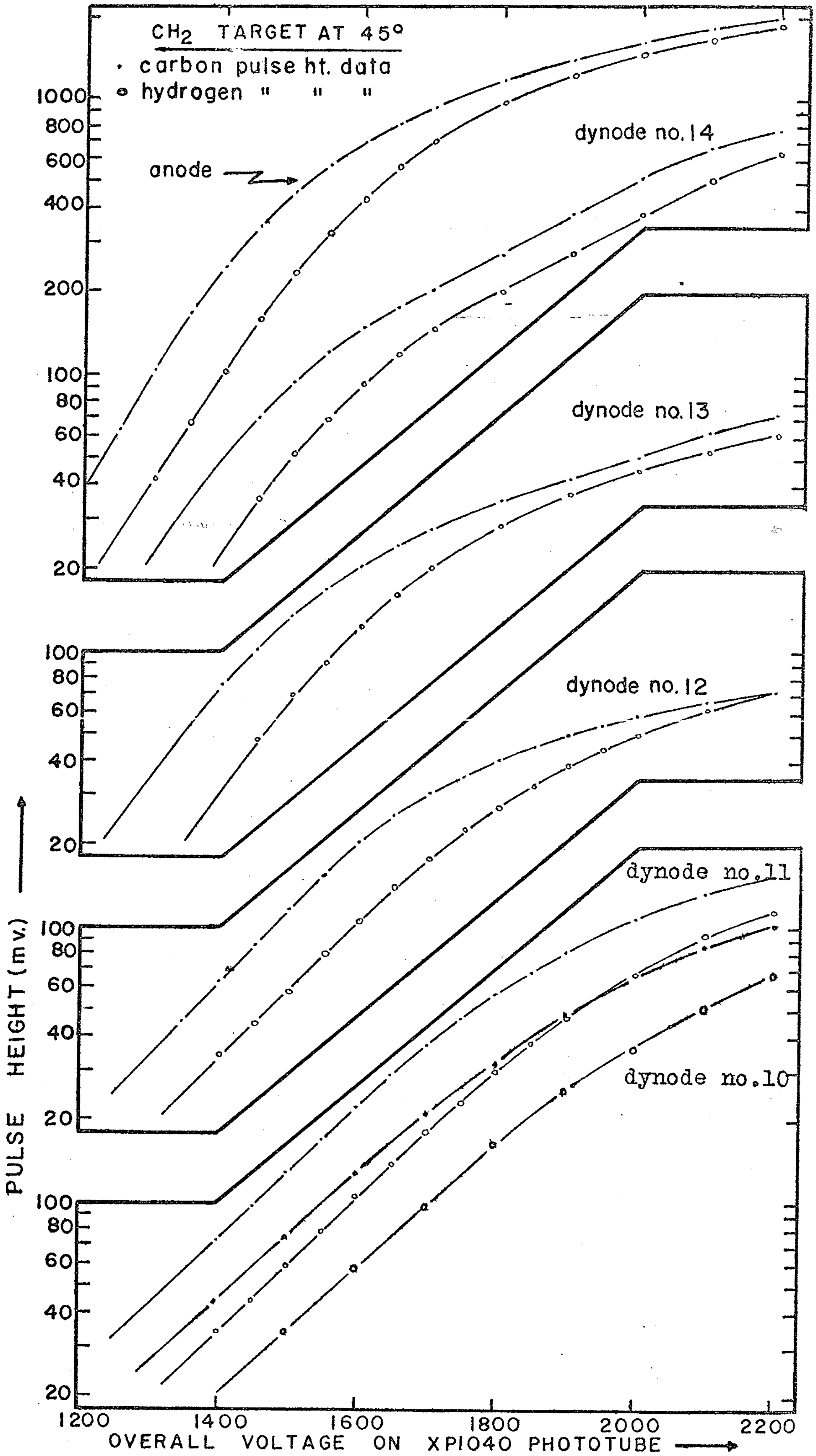

CH2 TARGET AT 45°
• carbon pulse ht. data
○ hydrogen " " "
anode
dynode no. 14
dynode no. 13
dynode no. 12
dynode no. 11
dynode no. 10
PULSE HEIGHT (mv.)
OVERALL VOLTAGE ON XP1040 PHOTOTUBE
1200
1400
1600
1800
2000
2200

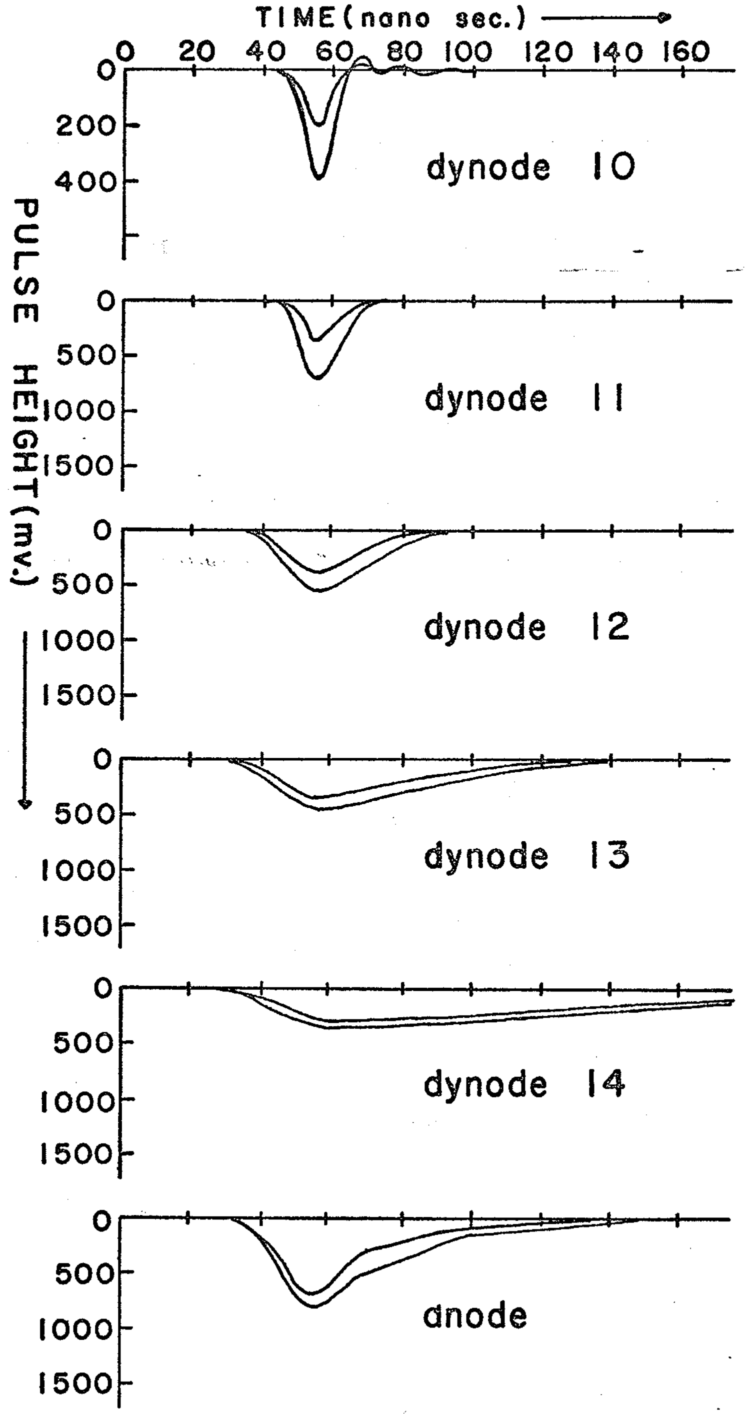

FIGURE 16

Pulse shapes from XP1040 phototube using the base circuit of Fig. 13 and an overall voltage of 1800 volts.

different cable from the one used with the EMI phototube). In order to find the effect of the space charge saturation on the charge of the dynode pulses, the charge of the carbon and hydrogen pulses (found from the area of the pulses in Figure 16) were plotted against the dynode number in Figure 17. Here, as before, the saturation effect can be seen in the change of slope of the lines.

From Figure 17 we can find the average currents delivered from the phototube for different count rates at the approximate overall voltage which we will be using in experiments with the spectrometer. At count rates of 10^5 per second we get an average current of about .3 ma, which is one tenth the value of the chain current, delivered from the anode of the phototube. At higher count rates the average current from the anode becomes comparable with the chain current and the need for the voltage stabilizing zeners becomes obvious.

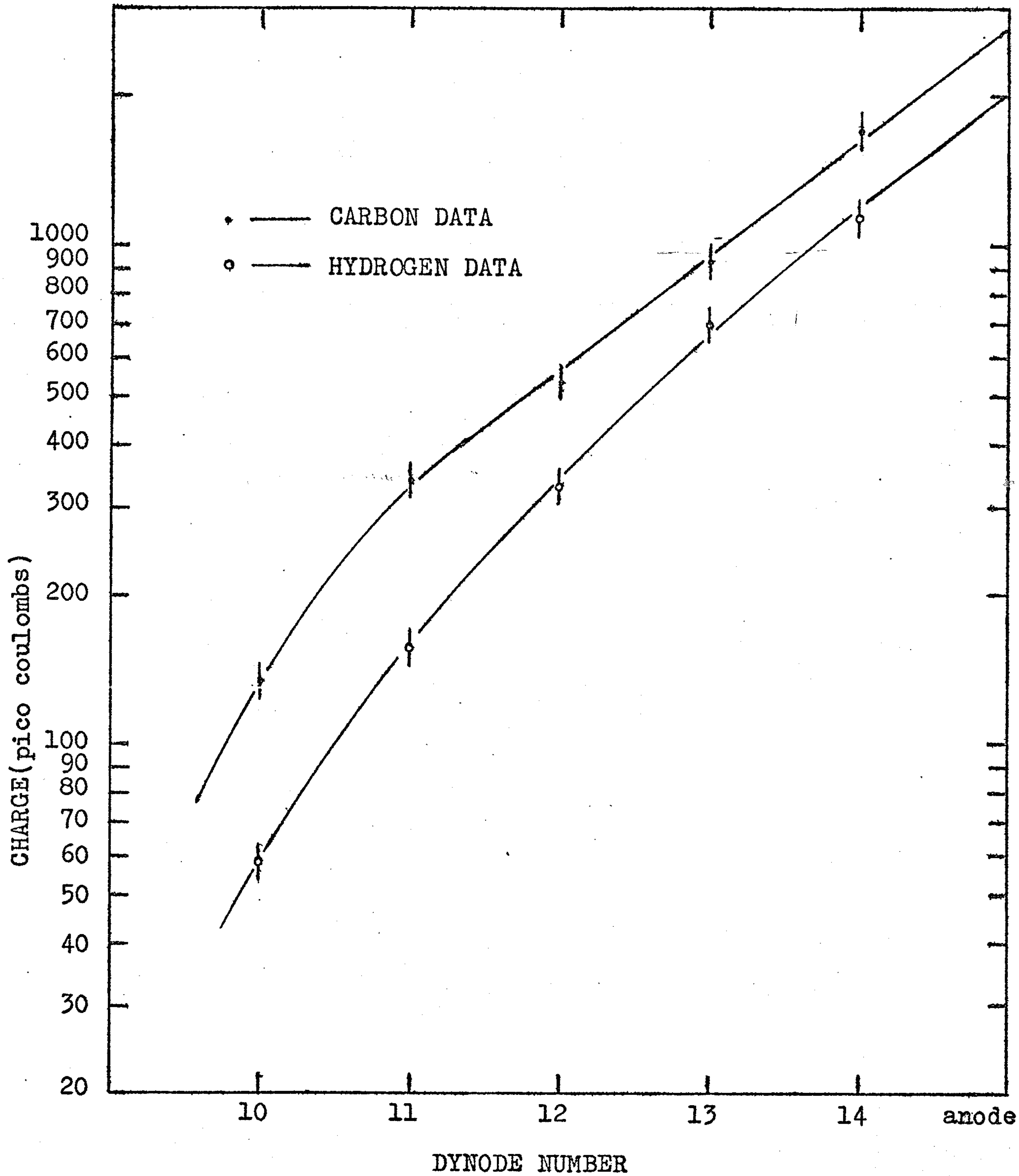

FIGURE 17

Charge of carbon and hydrogen pulses (calculated from the area of the pulses in Fig. 16) versus dynode number.

CHAPTER V

OVERALL PERFORMANCE OF COUNTERS

5-1 Linearity of Counters for 0-50 mev Protons

From the results of chapter lV it was possible to choose a base circuit, determine the dynode from which pulses could be taken for an energy measurement, and to find the approximate operating voltage for the phototube. After deciding on the above it was now necessary to test the linearity of the counters under normal operating conditions. This was accomplished by measuring the energies of the scattered protons from a polyethelene target in a 1024 multichannel analyser. The proton energies were varied from 25 mev to 50 mev by changing the incident beam energy and also by inserting aluminium absorbers (made from several layers of aluminium foil) in front of the counters. By using absorbers of thicknesses 5, 10, 20, 40 and 80 mils it was possible to observe protons with different energies below 25 mev. The results for one of the small counters is shown in Figure 18 for two different overall phototube voltages. Here the base circuit of Figure 10 was used with a chain current of approximately $5\frac{1}{2}$ ma and for the energy measurement pulses were taken from dynode number 11. The dynode pulses were inverted in a pulsetransformer (EG&G IT100) before sending them to the control room. From Figure 18 it can be seen that increasing the voltage on the phototube has the effect of saturating the pulses at a lower energy, as expected. However it

Figure 18

Channel number versus energy, for two overall phototube voltages, for the small counter.

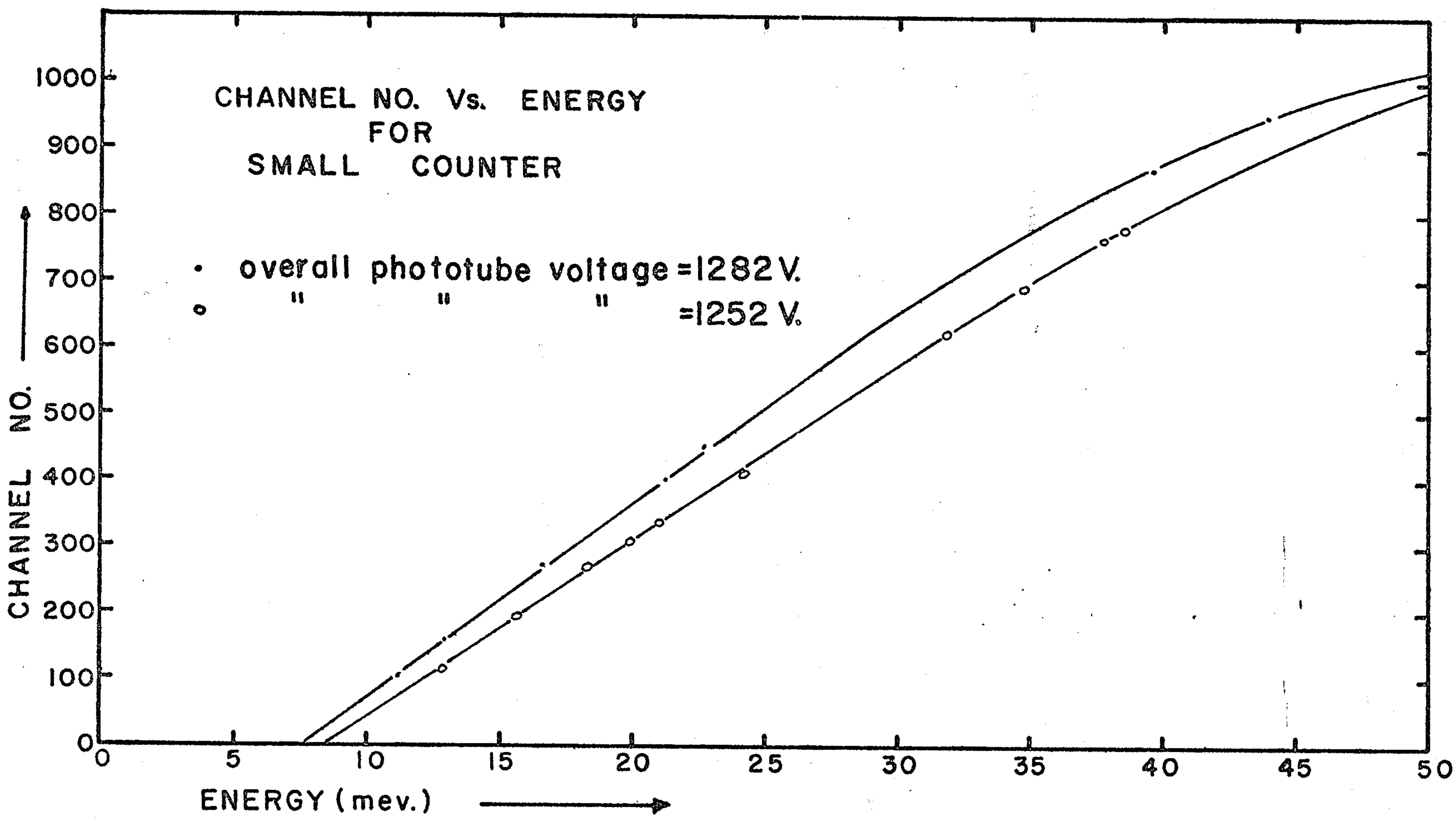

CHANNEL NO. Vs. ENERGY
FOR
SMALL COUNTER
• overall phototube voltage =1282 V.
o " " " =1252 V.
CHANNEL NO.
ENERGY (mev.)
0
100
200
300
400
500
600
700
800
900
1000
0
5
10
15
20
25
30
35
40
45
50

also reduces the cut off energy which may be important when the range of energies of interest are in the low energy region.

The results for one of the large counters, when the dynode 10 pulses from both top and bottom phototubes are inverted and added in a mixer module, are shown in Figure 19 Here the base circuit of Figure 13 was used with a chain current of approximately 3 ma and an overall operating voltage of around 1700 volts (1695v on top and 1671v on the bottom counter)

5-2 Spectra from CH_2 and Ta Targets for Collimated and Uncollimated Protons.

Using the scattering chamber of Figure 1 fitted with a movable target holder (not shown), spectra from a 6 mil CH_2 target and a 1 mil Ta target were observed. This was achieved by passing the pulses (the summed pulses in the case of the large counters) through a stretcher module and then via Nuclear Data ADC's into the memory of the PDP-9 computer. Using computer programs developed at the University of Manitoba the spectra were then plotted on a Calcomp plotter.

Typical collimated spectra at 45° from the 6 mil CH_2 target, for both small and large counters, at beam energies of arround 23 mev and 45 mev are shown in Figures 20 and 21 In both cases the scattered protons have been collimated at the centre of the scintillators by collimators of $\frac{1}{2}$ in and 1 in diameters for the small and large counters respectively. The resolutions of the carbon peaks for the small counter are 2.2% at 23 mev and 1.84% at 46.6 mev. The resolutions for the large counter are 4.3% and 3.5% respectively.

Figure 19

Channel number versus energy for large counter

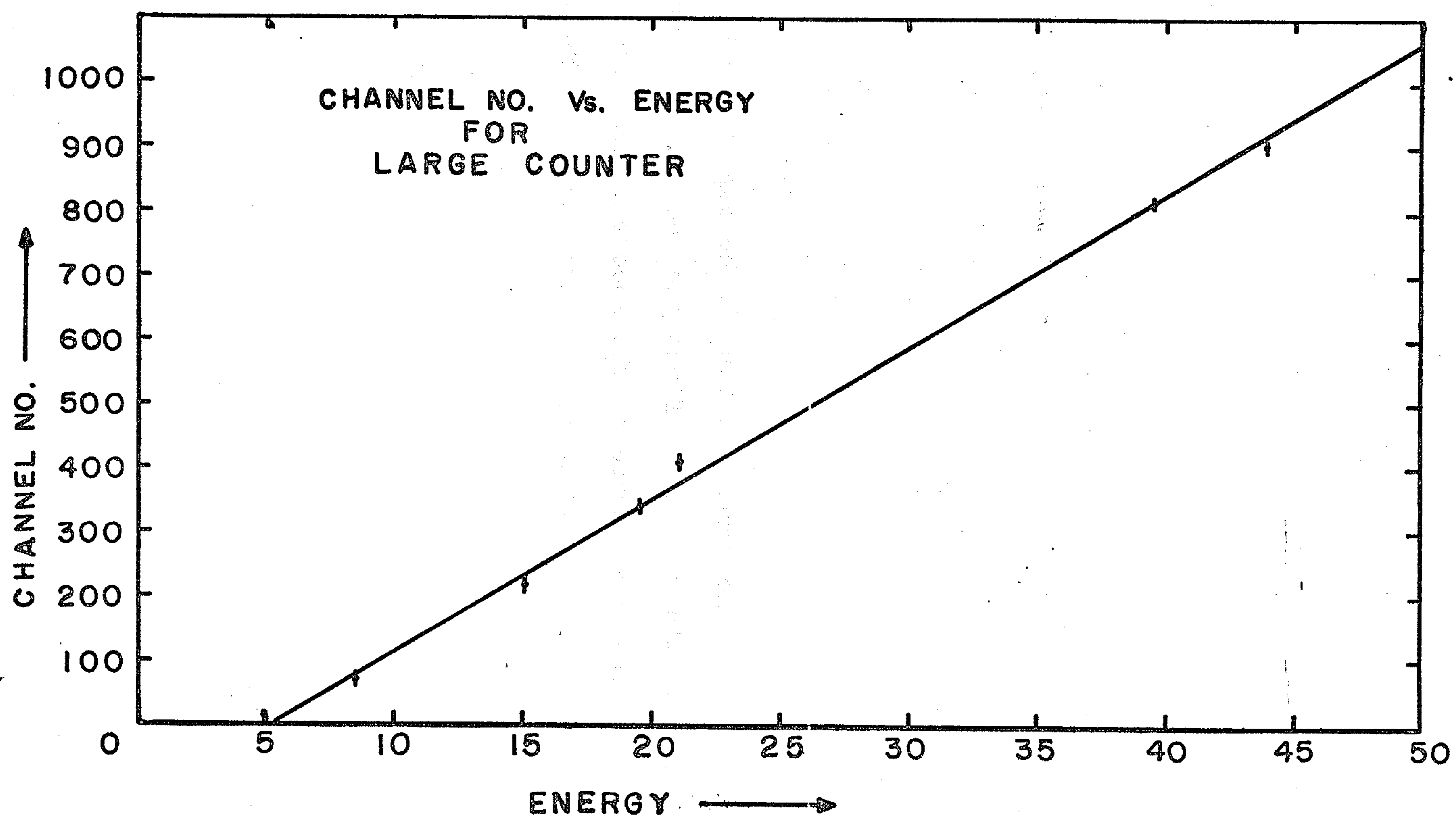
CHANNEL NO. Vs. ENERGY
FOR
LARGE COUNTER
CHANNEL NO.
ENERGY
1000
900
800
700
600
500
400
300
200
100
0
5
10
15
20
25
30
35
40
45
50

Figure 20

Typical spectra from a CH_2 target at incident beam energies of 23 mev and 46.6 mev for the small counter. The ground states of the carbon and hydrogen nuclei along with the first excited (4.4mev) states of carbon are marked on the spectra. The third excited state (9.6mev) of carbon is also marked at the higher energy.

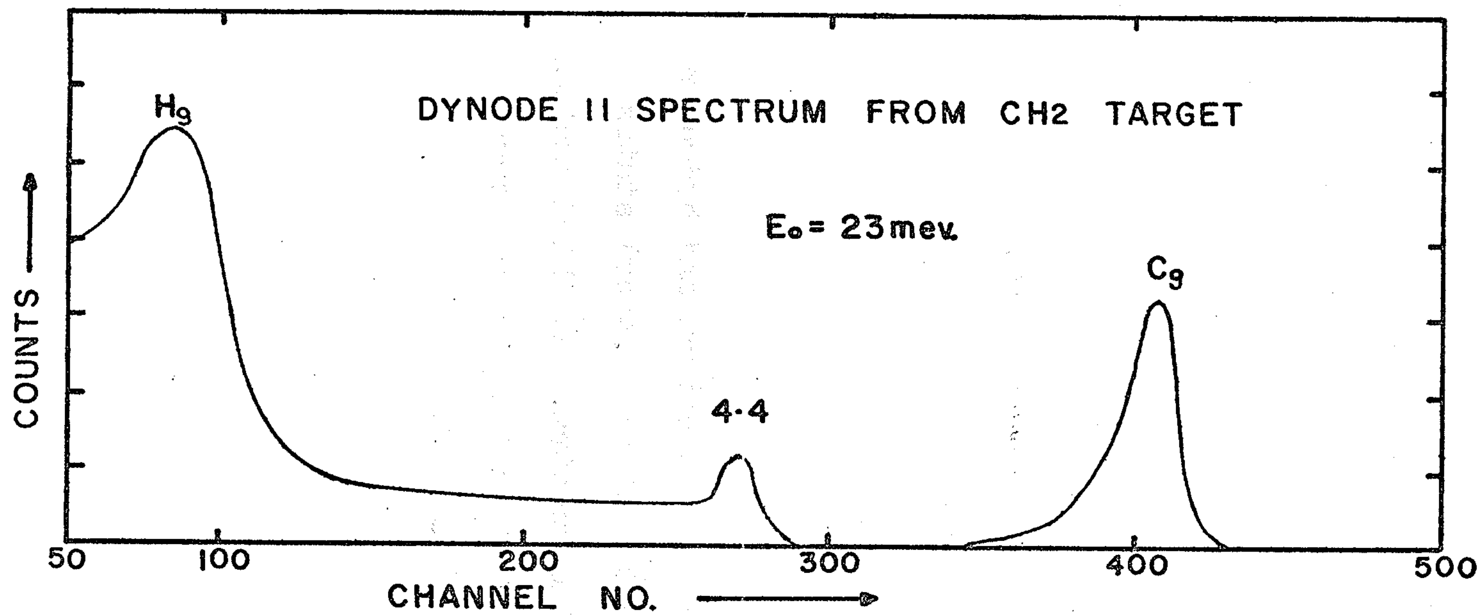
DYNODE II SPECTRUM FROM CH2 TARGET
E_o = 23 mev.
H_g
4·4
C_g
COUNTS
50
100
200
300
400
500
CHANNEL NO.

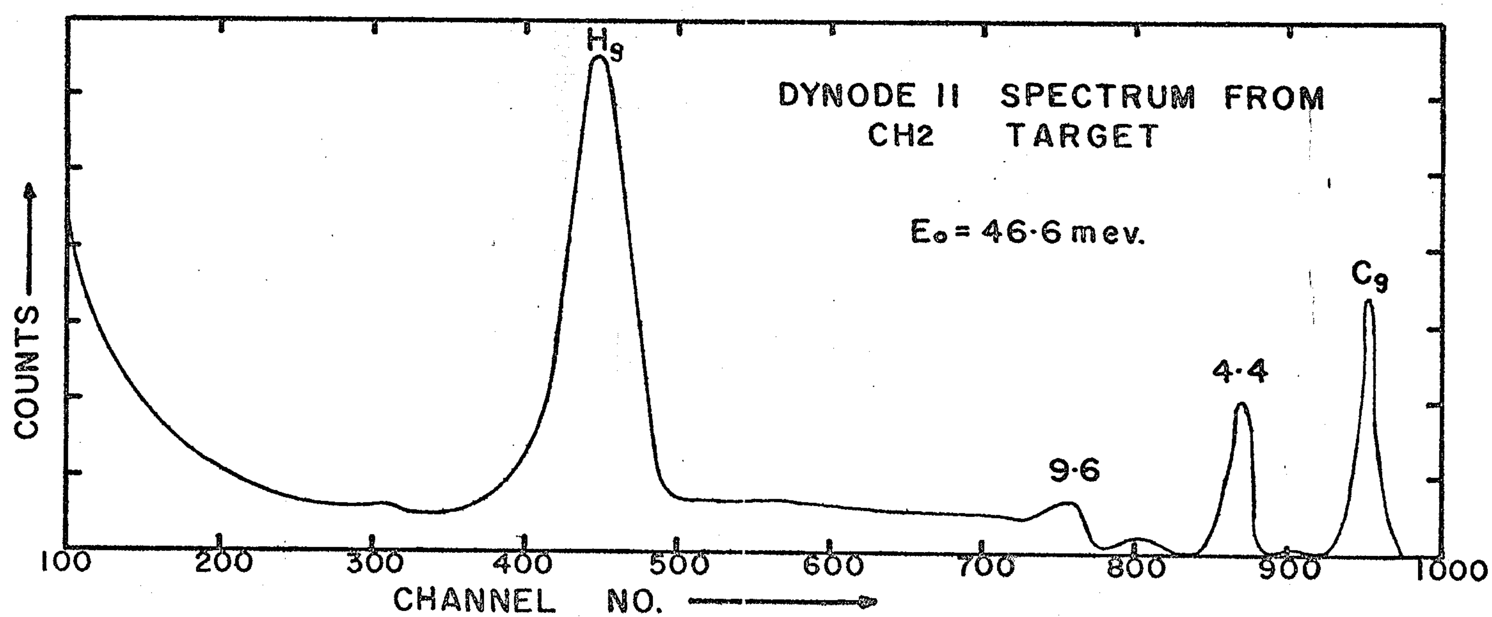
DYNODE II SPECTRUM FROM CH2 TARGET
E_o = 46·6 mev.
H_g
9·6
4·4
C_g
COUNTS
100
200
300
400
500
600
700
800
900
1000
CHANNEL NO.

Figure 21

Typical spectra from a CH_2 target at incident beam energies of 23.6 mev and 41.5 mev for the large counter. The ground states of the carbon and hydrogen nuclei along with the first excited (4.4mev) states of carbon are marked on the spectra. The third excited state (9.6mev) is also marked at the higher energy.

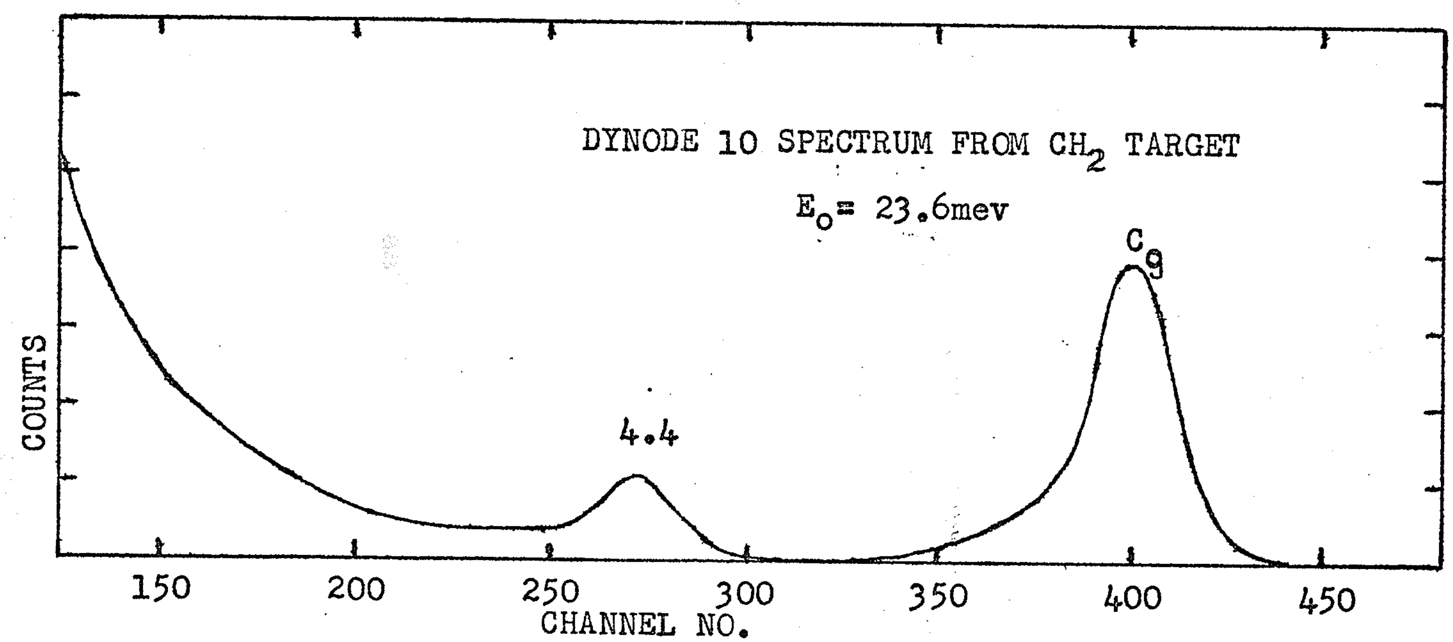
DYNODE 10 SPECTRUM FROM CH2 TARGET
Eo= 23.6mev
Cg
4.4
COUNTS
150
200
250
300
350
400
450
CHANNEL NO.

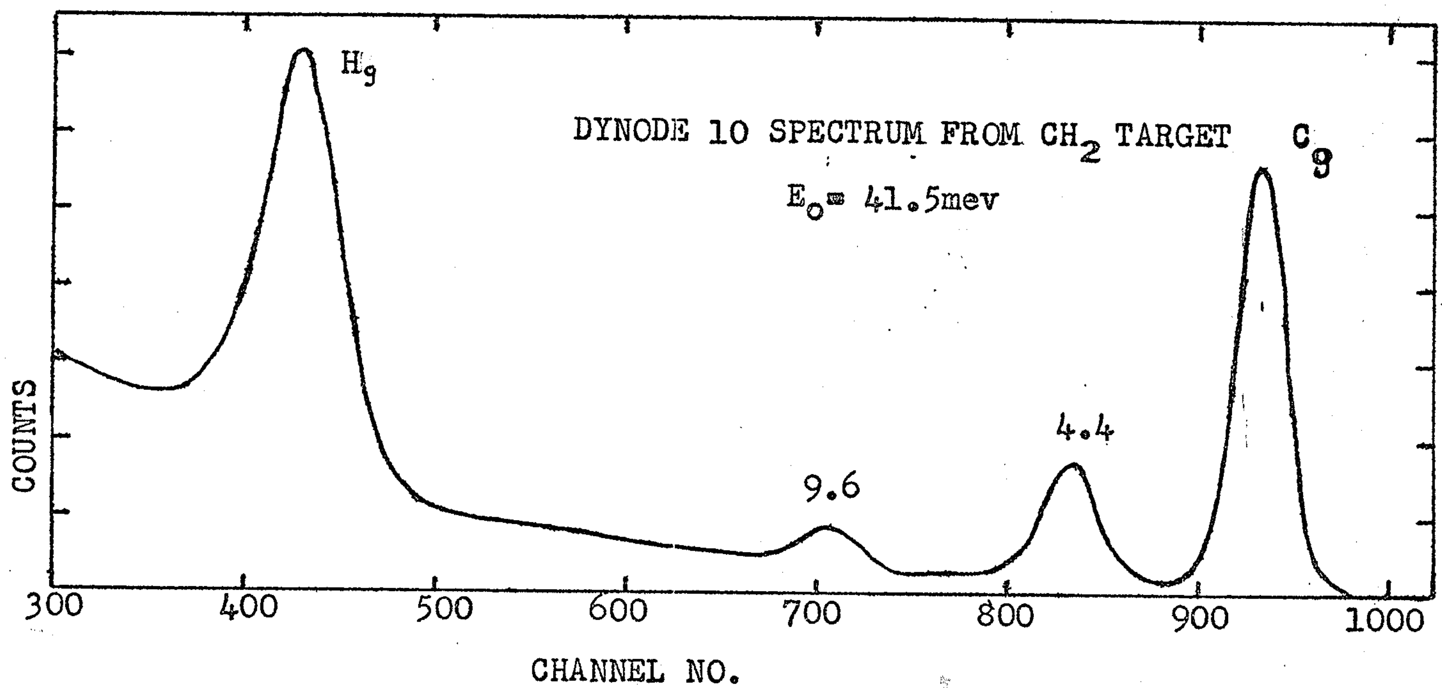
DYNODE 10 SPECTRUM FROM CH2 TARGET
Eo= 41.5mev
Hg
Cg
9.6
4.4
COUNTS
300
400
500
600
700
800
900
1000
CHANNEL NO.

The collimated and uncollimated spectra from the 1 mil thick Ta target for a beam energy of 42.2 mev are shown in Figure 22 for the small counter and in Figure 23 for the large counter. From the Figures the non-uniformity of the counters can be determined. In the case of the small counter shown here the non-uniformity, see page 5, is about 14% and for the large counter it is about 22%. Also from the Figures the collimated resolutions from the Tantalum target are 2.3% and 4.6% for the small and large counters respectively. The reason for the poorer resolutions, compared to that obtained using the CH_2 target, is due to the energy loss in the Ta target.

The results for the resolutions, from the Ta target, at different beam energies are shown in Figure 24. The measurements were taken using $\frac{1}{4}$ in and $\frac{1}{2}$ in diameter collimators for the small and large counters respectively. Straight lines obeying the $1/\sqrt{E}$ law have been drawn through the points.

5-3 <u>Method Used in Correcting Non-uniformity of Large Counters</u>

The non-uniformity of the large counters was determined by observing the pulseheights of scattered protons, collimated by a $\frac{1}{2}$ in diameter hole, from the Ta target at about thirty different positions across the face of the scintillator. The pulseheight at the centre of the scintillator was then divided by the pulseheights from these positions and the results plotted and interpolated onto a 10×10 correction matrix. The correction matrix was then stored in the memory of the 360/65 computer ready to be used along with a pulseheight correction (PHC) subroutine program to correct for the pulse-

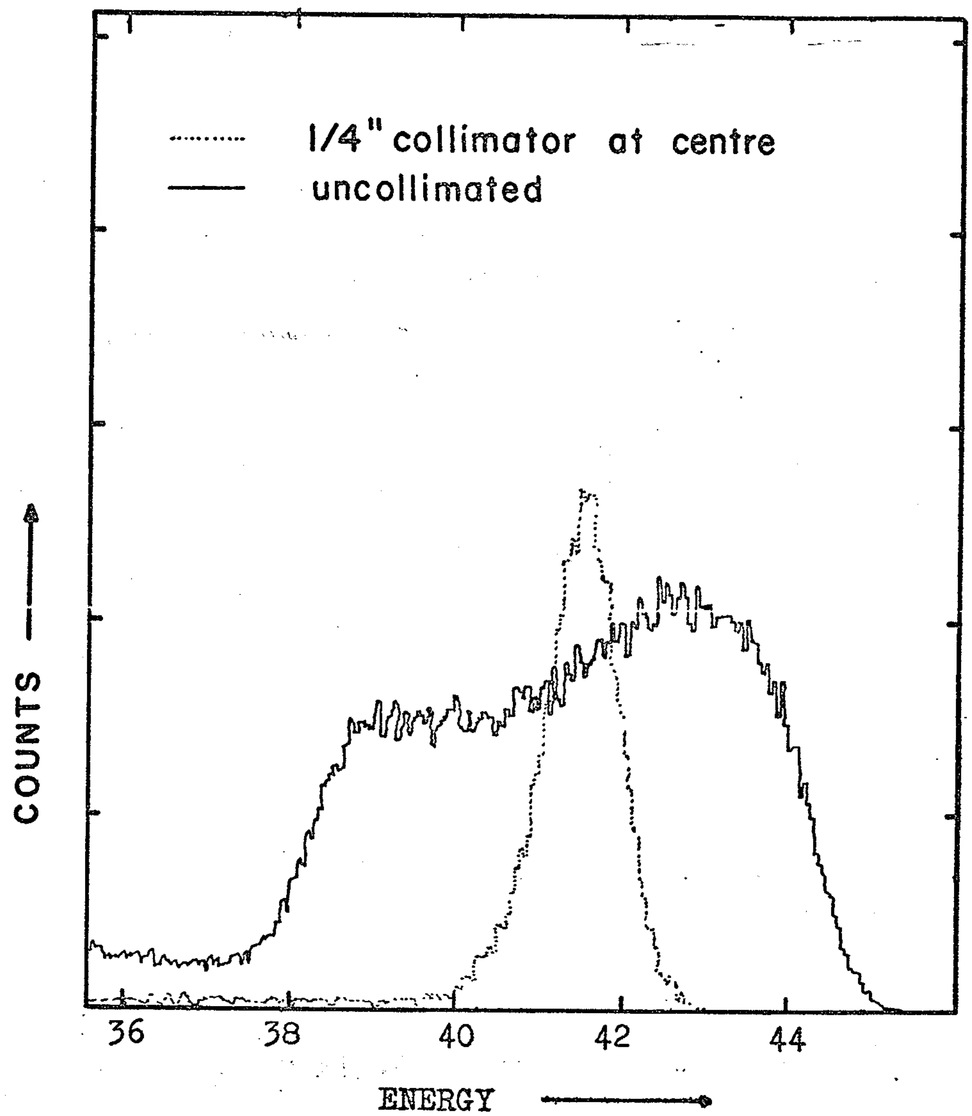

FIGURE 22

Ta spectra for the small counter showing the resolutions for the uncollimated and collimated cases.

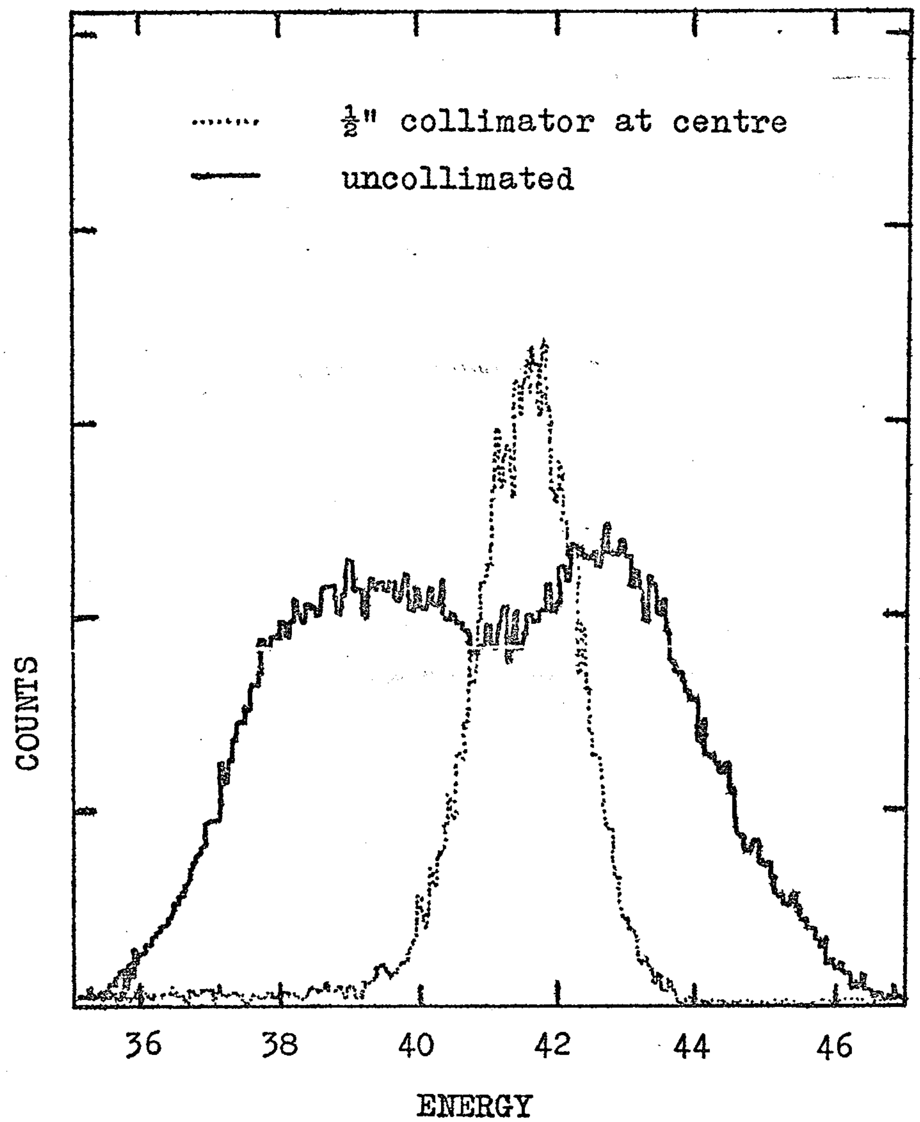

FIGURE 23

Ta spectra for the large counter showing the resolutions for the uncollimated and collimated cases.

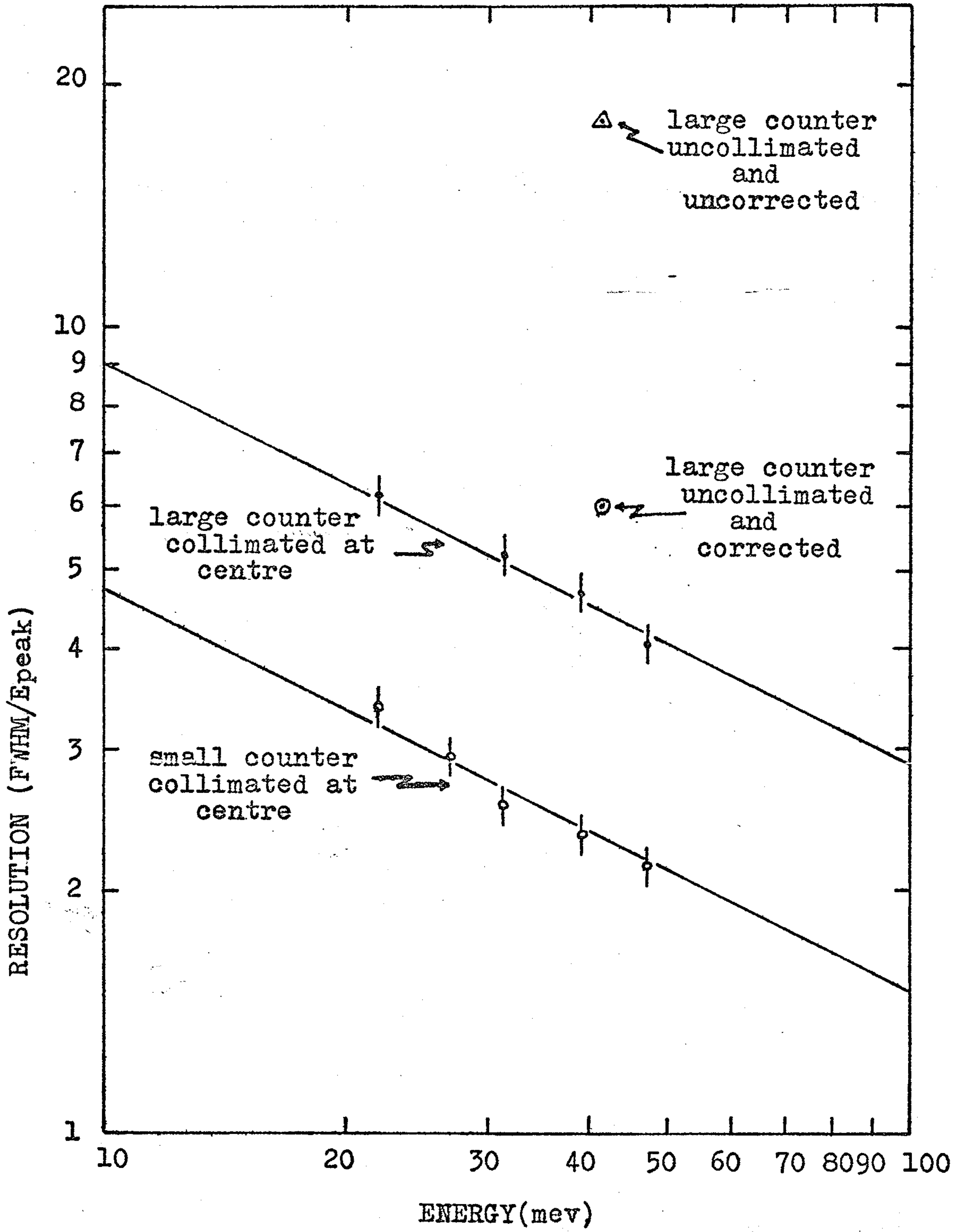

FIGURE 24

Resolution versus energy for both the small and large counters.

height non-uniformity.

In order to test the correction matrix, the wire chambers were sparked on random elastic coincidences from the Ta target, with the counters uncollimated, and the results, giving the spark co-ordinates and the proton pulseheights, stored on magnetic tape. The data was then processed off-line, using kinematic (which eliminate any background events) and related programs developed at the University of Manitoba, to give histograms of the pulseheight distributions for both of the large counters. In this manner it was possible to compare the spectra for the corrected and uncorrected pulseheights.

Another method for obtaining the distribution of pulseheights, and hence the correction matrix, is to ask the computer to separate the tantalum data into 'bins' where each bin gives the pulseheight distribution for a particular area on the face of the scintillator. The pulseheight corresponding to the peak of this distribution can then be taken as the average pulseheight for that particular area. The correction matrix can then be calculated as before. In order for this method to be sucessful it is necessary that each bin contains enough events (≥ 100) for the pulseheight at the centre of the distribution to be statistically significant. To get the 100 bins necessary to form the 10×10 correction matrix the wire chambers would have to be sparked approximately 100,000 times.

Due to time restrictions however, the wire chambers were sparked for only a fraction of this number and it was possible only to use the data to 'tune' the correction matrix already calculated by the first method described above. This was accomplished by finding the average pulseheights from only 16 different areas (instead of 100) on the scintillator. The uncorrected pulseheight at the centre of the scintillator was then divided in turn by the average pulseheights from the 16 different areas, which were corrected using the original 10×10 correction matrix, and arranged to form a 4×4 'tuning' matrix. The 4×4 tuning matrix was then interpolated to form a 10×10 tuning matrix and multiplied by the original 10×10 correction matrix to form a new 10×10 tuned correction matrix.

The correction matrices for both large counters, computed by the method described above, are shown in Figures 25a and 25b. From the Figures it can be seen that the largest variation in the non-uniformity occurs around the edges of the scintillator. This is particularly true in the case of the left counter where one of the light pipes coupled to the bottom face of the scintillator did not fit exactly onto the face but left a small triangular area through which the light may escape. The left counter was the one manufactured by our own workshop, and at the time of constructing it was thought that this area would only slightly affect the uniformity.

The correction matrices of Figures 25a and 25b were stored in the memory of the 360/65 computer and were ready to be tested using the Tantalum data. The results for the corrected and uncorrected pulseheights are shown in Figures 26a and 26b for the left and right counters respectively. The thick line represents the uncorrected spectra and the thin line the cor-

Figure 26a

Correction matrix for the large left counter

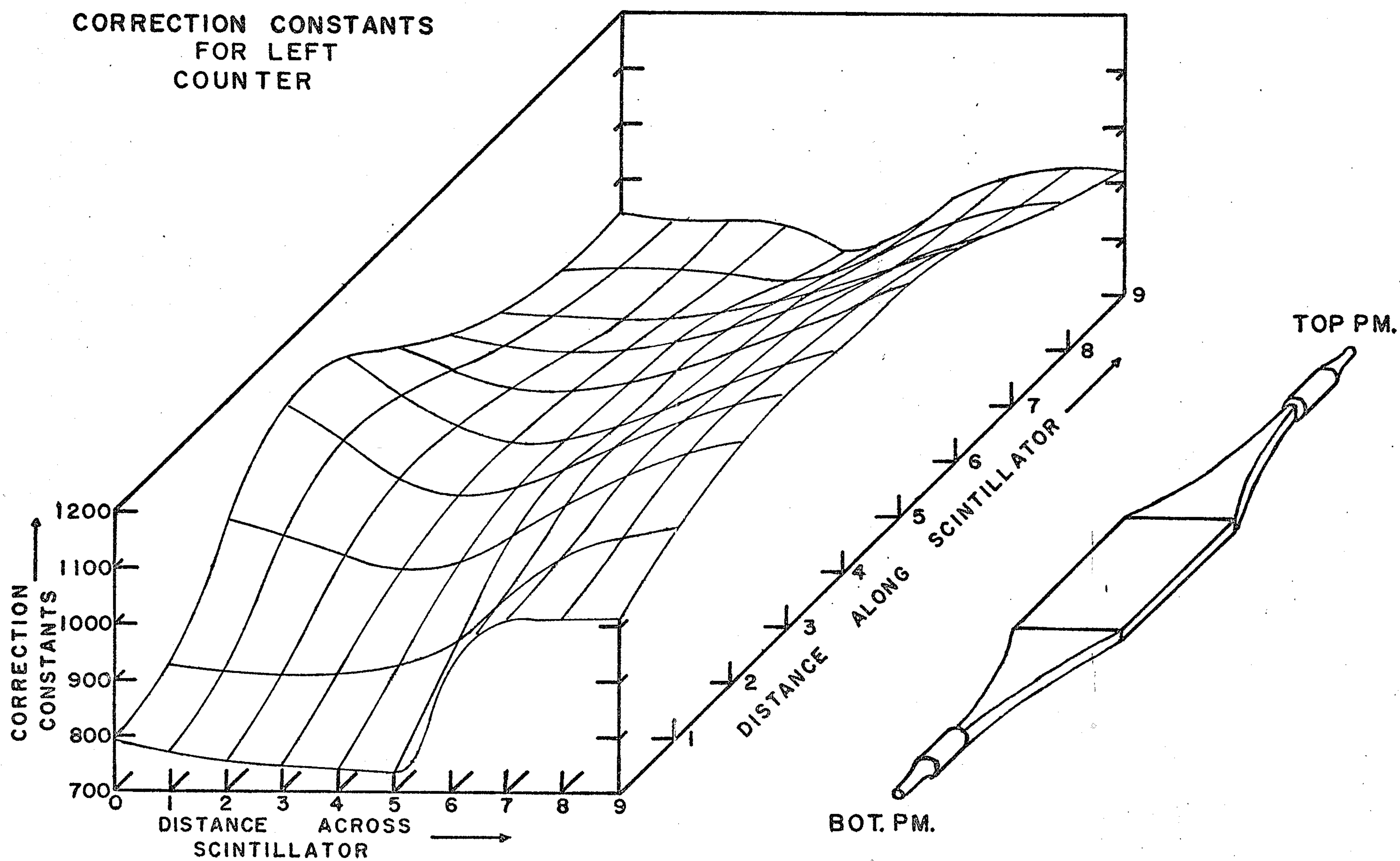

CORRECTION CONSTANTS FOR LEFT COUNTER
CORRECTION CONSTANTS
1200
1100
1000
900
800
700
0
1
2
3
4
5
6
7
8
9
DISTANCE ACROSS SCINTILLATOR
DISTANCE ALONG SCINTILLATOR
TOP PM.
BOT. PM.

Figure 26b

Correction matrix for the large right counter

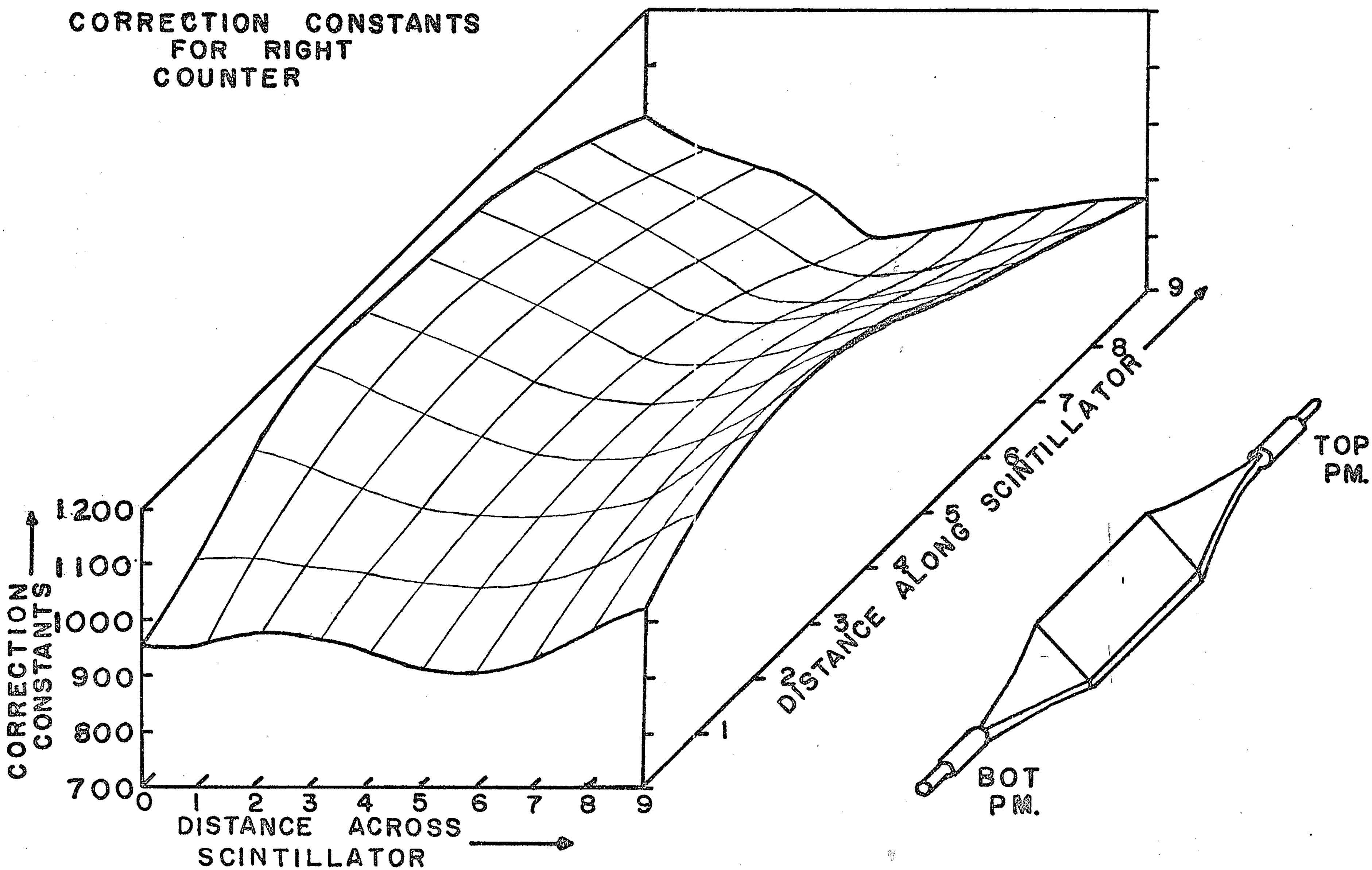

CORRECTION CONSTANTS
FOR RIGHT
COUNTER
CORRECTION CONSTANTS
1200
1100
1000
900
800
700
0
1
2
3
4
5
6
7
8
9
DISTANCE ACROSS SCINTILLATOR
DISTANCE ALONG SCINTILLATOR
TOP PM.
BOT PM.

Figure 27a

The uncorrected (heavy line) and corrected (thin line) spectra for the large left counter from a 1 mil Ta target, with incident beam energies of 41.4 mev.

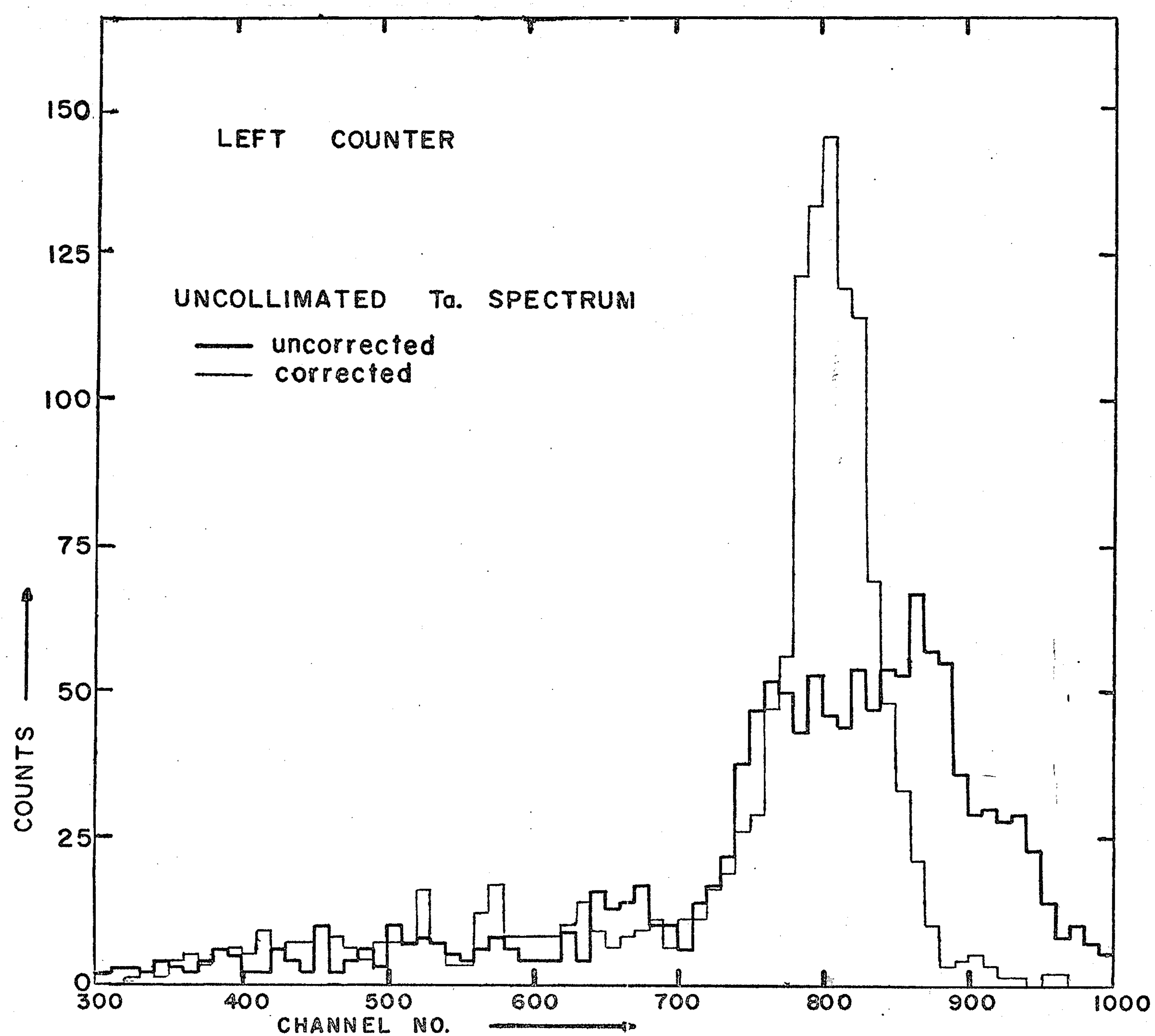
LEFT COUNTER
UNCOLLIMATED Ta. SPECTRUM
uncorrected
corrected
COUNTS
CHANNEL NO.
150
125
100
75
50
25
0
300
400
500
600
700
800
900
1000

Figure 27b

The uncorrected (heavy line) and corrected (thin line) spectra for the large right counter from a 1 mil Ta target, with incident beam energies of 41.5 mev.

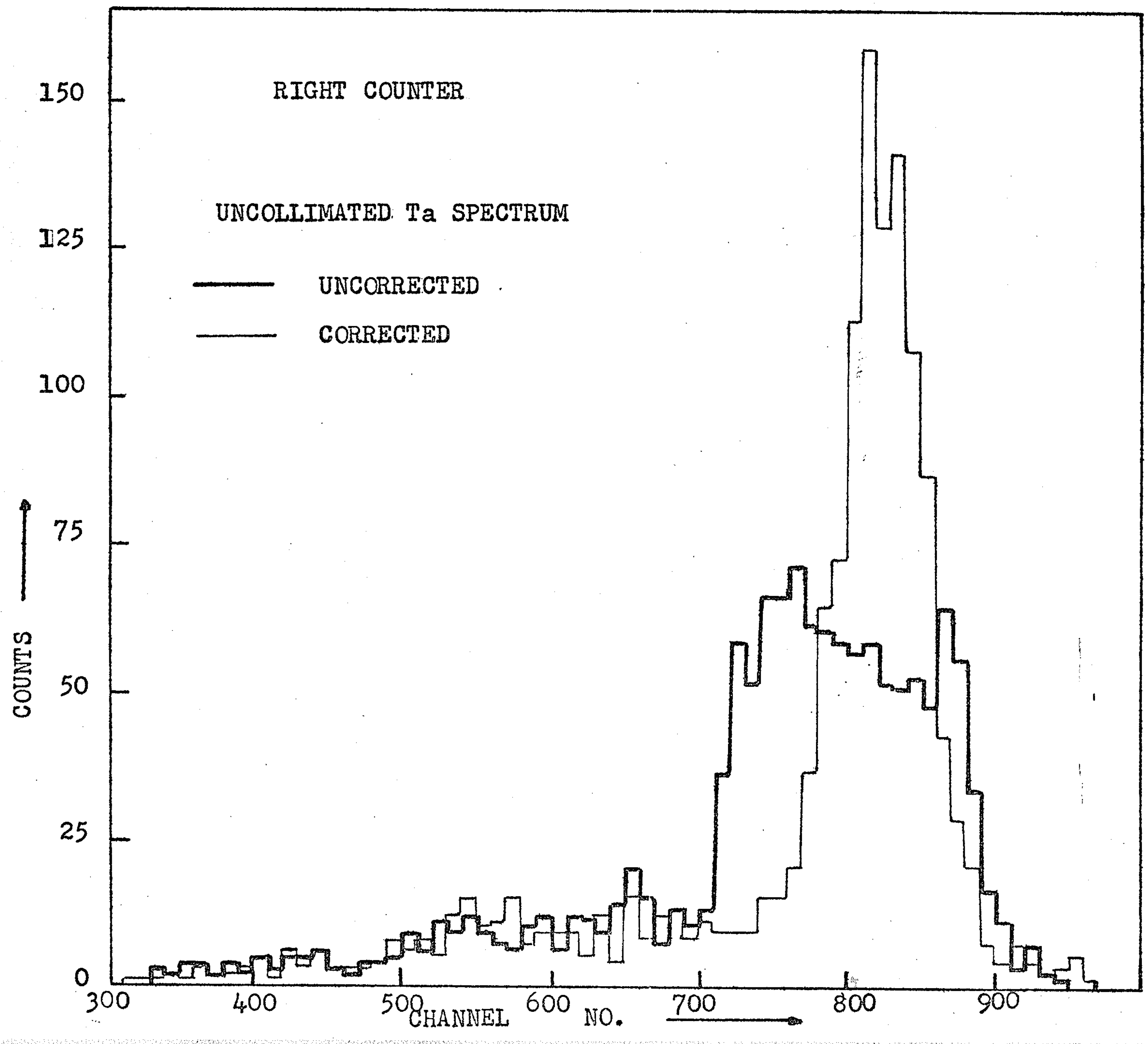
RIGHT COUNTER
UNCOLLIMATED Ta SPECTRUM
UNCORRECTED
CORRECTED
COUNTS
150
125
100
75
50
25
0
300
400
500
600
700
800
900
CHANNEL NO.

rected one. From the Figures it can be seen that the computer, by correcting the pulseheights, improves the resolution of the counters by a factor of 3, from 18% to 6% at an energy of 41.5 mev. It is hoped that by taking more of the Tantalum data it will be possible, due to better statistics, to improve the resolution even further.

CHAPTER VI

CONCLUSIONS

From the results of Chapter IV it appears that more work is necessary before the optimum base circuit for the EMI 9618R photomultiplier is obtained. The base circuit presented in Chapter IV for the Philips XP1040 photomultiplier is currently being used with the large counters in experiments using the wire chamber spectrometer.

The resolution of the large counters differ by a factor of two from that of the small counters, and this is qualitatively accounted for by the absorption of light in the scintillator and light pipes, and photomultiplier properties. The collimated resolutions for the large and small counters for protons scattered from the CH_2 target at incident beam energies of 46.6 mev are 1.84% and 3.5% respectively.

The uniformity and resolution of the large counters are seriously affected by small imperfections (1% of the total area) in the optical contact between the scintillator and light pipes, and consequently, the pulseheights from around the edges of the scintillator account for a large part of the non-uniformity. Taking into account these effects, the pulse-height non-uniformity for the large counters was as much as 25%. Measurements of the non-uniformity from the uncollimated Ta target (which tend to average out any local effects) give values for the non-uniformity of 12.5% for the small counters.

By using the information from the wire chambers it is possible to correct for the pulseheight non-uniformity. The results so far have shown that the overall resolution of the large counters can be improved by a factor of three, and that further improvement can be expected by increasing the amount of Ta data. Overall resolutions of between 3.5% and 4% at energies around 45 mev can be expected in the near future.

APPENDIX

DESCRIPTION OF THE PULSEHEIGHT CORRECTION PROGRAM (PHC)

The purpose of the PHC program is to correct the pulseheights of protons which pass through the wire chambers and strike the scintillators. The program requires the following input information:

1) The angles, theta, which the protons make with the beam direction, and phi, the projected angle normal to the beam direction.
2) The co-ordinates (x,y) of the rear wire chambers (with the origin at the edge of the chamber).
3) The pulseheight Po of the particle to be corrected.
4) The set C(i,j) of calibration points (i.e. the 10X10 correction matrix).
5) The distance, d between the scintillator and the rear wire chamber.

The first thing the program does is to re-scale the co-ordinates of the wire chambers, which have the range 0-324 and are in 1/40 inch units, into one inch units and shift the origin to the centre of the wire chambers.

Next we have to correct the parallax between the rear wire chamber and the scintillator. The parallax is caused by the finite distance (d) between the rear wire chamber and the face of the scintillator and is corrected by using the angles Φ and θ.

i.e.
$$x' = (x - 162)/40 + \mathrm{SIN}(\theta)\mathrm{COS}(\Phi)$$
$$y' = (y - 162)/40 + \mathrm{SIN}(\theta)\mathrm{SIN}(\Phi)$$

The range of the co-ordinates, x', y' are $-4\frac{1}{2}''$ to $-4\frac{1}{2}''$ and by adding $5\frac{1}{2}''$ we can get the more suitable range of 1-10 which corresponds to the range of the correction matrix.

We are now ready to correct the pulseheight of the particle by multipling it with a correction constant found from an interpolation of the 10×10 correction matrix. By separating the x and y co-ordinates into integer and decimal parts, i.e.

$x = I + R$ (where I is an integer, and R is decimal)

and knowing the calibration points;

$$C1 = C(i,j) \quad , \qquad C2 = C(i+1,j) \; ,$$
$$C3 = C(i,j+1) \; , \qquad C4 = C(i+1,j+1) \; ,$$

we can proceed to form a four way interpolation between them i.e.

$$C12 = C1 + (C2-C1)\times R1$$
$$C13 = C1 + (C3-C1)\times R2$$
$$C24 = C2 + (C4-C2)\times R2$$
$$C34 = C3 + (C4-C3)\times R1$$

where R1 and R2 are the decimal parts for the x and y co-ordinates resp.

Next we interpolate between C24 and C13, and C34 and C12 i.e.

$$Cv = C12 + (C34-C12)\times R1$$
$$Cq = C13 + (C24-C13)\times R2$$

and finally by averaging the Cv and Cq we get the correction factor H, which when multiplied by the pulseheight Po of the particle corrects for the pulseheight non-uniformity, i.e.

$Pc = Po\times H$ where Pc is the corrected pulseheight.

Listing of PHC

```
      SUBROUTINE PHC (PHT,PHTC,X,Y,ATHETA,PHI,C,D,)
      DIMENSION C(10,10)
      A=X
      B=Y
      THETA =ATHETA - 32.5*3.14159/180
      X=(X-162.)/40.+SIN(THETA)*COS(PHI)*D 5.5
      Y=(Y-162.)/40.+SIN(THETA)*SIN(PHI)*D 5.5
      IF(X.LT.1.) GO TO 200
      IF(X.GE.10) GO TO 200
      IF(Y.LT.1.) GO TO 200
      IF(Y.GE.10) GO TO 200
  100 I=X
      J=Y

      R1=X-I
      R2=Y-J

      C1=C(I,J)
      C2=C(I+1,J)
      C3=C(I,J+1)
      C4=C(I+1,J+1)

      C12=C1+(C2-C1)*R2
      C34=C3+(C4-C3)*R2
      CV=C12+(C34-C12)*R1

      C13=C1+(C3-C1)*R1
      C24=C2+(C4-C2)*R1
      CQ=C13+(C24-C13)*R2

      H=(CV+CQ)/2.

      PHCT = PHT*H
  200 X=A
      Y=B
      RETURN
      END
```

REFERENCES

1. L.G. Greeniaus et al, Proc. of Int. Symposium on Nucl. Electronics, Versailles, Sept. 1968, Vol. 3, p. 56

2. D. Brini et al, Nuovo Cim. 2 Suppl. (1955), 1048

3. M.A. Meyer and N.S. Wolmarans, Nucl. Instr. and Meth. 25 (1963) 134

4. W.A. Gibson, Rev. Sci. Instr. 35, (1963) 1021

5. P. Gorenstein and D. Luckey, Rev. Sci. Instr. 34 (1963) 196

6. D.C. Crabb et al, Nucl. Instr. and Meth. 45 (1966) 301

7. PH. Catz, Nucl. Instr. and Meth. 56 (1967) 74

8. P.K.F. Grieder, Nucl. Instr. and Meth. 55 (1967) 295

9. B. Gottschalk, Rev. Sci. Instr. 40 (1969) 22

10. S. Donati et al , Nucl. Instr. and Meth. 46 (1967) 165

11. M.A. El-Wahab and M. Gazzaly, Nuovo Cim. Vol. XLVII B, N.1 (1967) 56

12. Yu. K. Akimov, Scintillation Counters in High Energy Physics, p. 13 (Academic Press, 1965)

13. M. Cocchi and A. Rota, Nucl. Instr. and Meth. 46 (1967) 136

14. R. Euling, J. Appl. Phys. 35 (1964) 1391

15. W.A. Shurcliff and R.C. Jones, Journ. Opt. Soc. Am. 39 (1949) 912

16. D. Brini et al, Nuovo Cim. 11 (1954) 655

17. R.L. Garwin, Rev. Sci. Instr. 23 (1952) 755

18. H. Hinterberger and R. Wiston, Rev. Sci. Instr. 39 (1968) 419

19. H. Hinterberger and R. Wiston, Rev. Sci. Instr. 37 (1966) 1094

20. D.E. Williamson, J. Opt. Soc. Am. 42 (1952) 712

21. P. Mockett, Rev. Sci. Instr. 35 (1964) 238

22. N.W. Reay and L.M. Preston, Rev. Sci. Instr. 35 (1964) 519

References- cont.

23. A. Stub, Rev. Sci. Instr. 35 (1964) 1268

24. M.S. Cook, Rev. Sci. Instr. 35 (1964) 920

25. C.Y. Fan, Rev. Sci. Instr. 35 (1964) 158

26. Nuclear Enterprises Inc., 935 Terminal Way, San Carlos, California, 94070

27. Technical data provided by Nuclear Enterprises Inc.

28. H.G. Evans and E.H. Bellamy, Proc. Phys. Soc., 74 (1959) 483

29. General Electric Siliqone Products Dept., Waterford, New York

30. T. Bowen, E.P. Krider and J. W. York, Nucl. Instr. and Meth. 50 (1967) 349

31. W.J. McDonald and D.A. Gedcke, Nucl. Instr. and Meth. 55 (1967) 1

32. H.J. Lush, J. Sci. Instr. 42 (1965) 597

33. EMI brochure, ref. 30M/6-67(PMT), issue 1

34. Amperex Catalog, Oct. 1955